Dynamic Simulation and Parametric Analysis of Solar Assisted Desiccant Cooling System with three Configuration Schemes

Abdul Samad Farooq [a], Abdul Waheed Badar [b*], Muhammad Bilal Sajid [a], Mahreen Fatima [a], Anam Zahra [a], M. Salman Siddiqui [c]

[a] *US-Pakistan Center for Advanced Studies in Energy, National University of Sciences and Technology, Islamabad, Pakistan.*
[b] *Department of Mechanical Engineering, HITEC University, Taxila, Pakistan.*
c Department of Architecture & Technology, Norwegian University of Science and Technology, NO-7491 Trondheim, Norway.

[*]Corresponding author. Tel.: +92 51 4908146-50, *E-mail address*: abdul.waheed@hitecuni.edu.pk

Abstract

Evaporative cooling of the dehumidified air in a desiccant cooling system with the aid of solar energy is an attractive energy saving option to cool the process air for air conditioning purposes. This paper is concerned with the dynamic simulation and performance analysis of three configuration schemes of a solar-based ventilation mode desiccant cooling system energized by a photovoltaic-thermal (PV/T) solar collector for the weather conditions of Lahore (31.52° N, 74.36° E). In configuration-1 (C-1), the auxiliary heater is installed in the air conditioning loop to heat the return air up to the desired regeneration temperature. In configuration-2 (C-2), the auxiliary heater is installed in the solar heating loop to raise the temperature of the liquid water to a certain high temperature. The configuration-3 (C-3) is similar to C-2 except there are no evaporative coolers and all the cooling is achieved via conventional vapor compression chiller. The primary energy savings, solar fraction, and the thermal efficiency of the solar collector are the energetic performance parameters which are used to compare the performance of three configuration schemes and to analyze the influence of various parameters such as regeneration temperature, solar collector size and tilt, flow rates, and storage volume. The simulation results demonstrated that the C-1 scheme performs best in terms of solar fraction and primary energy savings while C-3 schematic resulted in the least values of primary energy savings.

Keywords: Solar energy; PV/T; Desiccant cooling; TRNSYS; Primary energy savings.

---

1. Introduction

According to the International Institute of Refrigeration 15 % of the total electricity produced in the world is consumed for the refrigeration and air-conditioning and about 45 % of the total energy consumed by the commercial buildings and residences is used for air-conditioning and the demand is increasing continuously [1] [2]. Moreover, the concerns about the environmental impact of greenhouse gases (GHG) is also increasing [3]. Solar assisted air conditioning systems are one of the most attractive and reliable ways to mitigate environmental and power-related issues. Solar based cooling systems are broadly classified as electricity and thermal driven systems [4]. Solar thermal powered air conditioning systems currently in practice are mainly either absorption, adsorption, or desiccant based cooling systems. Utilization of low-grade energy, less dependence on non-natural working fluids and low to medium regeneration temperature requirement are the main benefits of the solar-based desiccant cooling system. Moreover, accommodation of latent and sensible loads separately makes it unique when compared to other air conditioning technologies. Desiccant material in a desiccant wheel plays a vital role in the accommodation of latent load. It may be in liquid or solid state and is used to absorb or adsorb the water vapors from the air due to the difference between the vapor pressure of water on the desiccant surface and the ambient air while rotating at a speed in the range of 8-10 rph [5]. The efficiencies of desiccant cooling systems in comparison to absorption systems are also expected to increase in the years to come [6].

Sheridan and Michell [7] designed a hybrid desiccant cooling system for the climatic conditions of Darwin in Australia and the objective was to investigate the energy saving in the hybrid system as compared to the conventional vapor compression system. Results show that depending upon the weather conditions hybrid system can save 25-40% more energy as compared to the conventional system. Subramanyam et al. [8] investigated the use of the desiccant wheel for air conditioning systems to control the desired humidity level and the performances of desiccant-based and conventional vapor compression air conditioner are analyzed and compared. Results show that the desiccant systems increase the dehumidification rate while COP decreased only by 5% as compared to the conventional air conditioner. Khalid et al. [9] designed a solar-assisted desiccant cooling model in TRNSYS for four different modes by using direct and indirect evaporative coolers for the climatic conditions of Karachi and Lahore in Pakistan and energy payback period for a solar collector was found to be 1.53Years. Al. Alili et al. [10] designed a desiccant based air conditioning system by using PV/T collectors for the climatic conditions of Dubai, U.A.E and unlike conventional desiccant system, all the cooling is achieved by using the vapor compression chiller. Ronghui et al. [11] analyzed the desiccant based air conditioning system for the climatic conditions of Singapore, Houston, Beijing, Los Angeles, and Boulder. The results show that more electrical savings can be achieved in the areas of high humidity and low sensible heat ratio. The lowest payback period was estimated to be 7 years for Singapore while the highest payback period of 30 years was found to be for Beijing. Ge et al. [12] studied the performance of two-stage rotary desiccant air conditioning system with varying regeneration temperatures. The results demonstrated that two different regeneration temperatures are to be employed for the two stages of the desiccant wheels with intercooling to achieve higher efficiency. Angrisani et al. [13] examined the desiccant cooling system with three different configurations for the climatic conditions of Italy and compared the performance with the conventional air conditioning system. It was found that by the use of the desiccant wheel as a dehumidifier 20-25 % primary energy savings can be achieved while CO_2 emissions can also be reduced up to 35-40 %. Elmer et al. [14] studied the desiccant air conditioning system for a building with a cooling capacity of 1362 W and potassium formate is used as a desiccant working fluid. Thermal COP of the given system was determined to be 1.26 while the electrical COP was found to be 3.67. A dynamic analysis of a solar desiccant cooling system was done by Heidari et al. [15] to produce the cooling effect as well as water for domestic use to address the issue of high water consumption of these systems. Buker et al. [16] experimentally studied a liquid desiccant cooling system in combination with the evaporative cooler and powered by a PV solar panel along with a polyethylene heat exchanger which was attached at the bottom of the PV panel for thermal energy extraction. Their results showed a significant performance improvement of the PV panels due to the extra heat dissipation to the flowing cold water in the heat exchanger loop.

There is a consistent need to further improve the overall system performance, particularly, of the small-scale solar cooling systems in terms of energy savings by further optimization and by introducing novel design concepts to make it competitive with conventional cooling systems. One of the ways is to study and analyze various possible system configurations of the thermally driven solar-based cooling system [17] [18] and to suggest the best configuration scheme based on key performance indicators. Due to the low to medium temperature requirements (50-90 ^{o}C) for the operation of solar-based desiccant cooling systems, PV/T solar collectors can be employed [10] as it is capable of simultaneously meeting the electrical as well as thermal loads. There is still room to investigate and compare the performance of the different possible versions of the system's schematics of solar desiccant cooling systems depending upon the type and specific connection arrangement of individual components of the system for improved primary energy savings. The objective of this study is to model, simulate and optimize a desiccant based air conditioning system in ventilation mode for the climatic conditions of Lahore (31.52° N, 74.36° E). The system is arranged in three different configuration schemes and energized by a flat plate PV/T solar collector. The dynamic analysis of the systems is performed in TRNSYS which is a convenient simulation tool for conducting off-line experimentation of novel energy concepts. Two system configuration-schemes (C-1, C-2) of the solar-based desiccant cooling systems employ direct and indirect evaporative coolers (DEC and IDEC) as the primary cooling devices while vapor compression chiller (VCC) is used as the auxiliary cooling source. C-1 differs from C-2 in the manner that auxiliary heater is installed in the return air of the air conditioning loop in the former case while in the latter case the auxiliary heater is installed in the solar water heating loop. The configuration-3 (C-3) is similar to C-2 except for vapor compression chiller (VCC) is used as the main cooling source as studied by Al Alili et al. [10]. System performance indicators that are used to compare the energetic performance of system schemes are thermal and electrical solar fractions, primary energy savings and efficiency of the PV/T solar collector. The influence of various design parameters such as the regeneration temperature, fluid flow rate, size and slope of the PV/T solar collector, and volume of the storage tank is also analyzed to optimize the system design.

2. Description of Simulated Systems

The desiccant cooling system uses the principle of alternate dehumidification and humidification of the process and regenerated air to achieve the desired cooling demand. A desiccant cooling system typically consists of two main loops. One loop is concerned with the treatment of the air to deliver it to the conditioned space at the desired temperature and humidity, thus can be regarded as the air-conditioning loop. This loop comprises of a desiccant wheel which absorbs the moisture from the process air, fan/blower, heat exchanger (s), direct/indirect evaporative coolers, auxiliary cooling source, and controllers (see Figs. 1 and 2). The operation of such ventilation mode desiccant cooling systems with reference to temperature and humidity variation is explained in [19]. The second loop is responsible for the generation of heat energy to dissociate the moisture absorbed by the desiccant wheel from the process air, thus can be referred to as heat generation loop. This can be achieved by supplying thermal energy from a conventional boiler and/or solar thermal collector to the return air before entering the desiccant wheel. A solar water heating system is normally employed to furnish the purpose of regeneration of desiccant wheel

The schematic layouts of the three configuration schemes (C-1, C-2, and C-3) of the solar-based desiccant cooling system to meet a peak cooling demand of 2.5 TR are described in Figs. 1-3. PV/T solar collector is utilized in all configuration schemes to generate energy from the sun in the form of heat and electricity which is to be stored in a stratified storage tank and in the electric battery, respectively. The stored electrical energy is subtracted from the total electrical energy consumption to run the auxiliary cooling device based on conventional vapor compression chiller to cool the process air to the desired room air temperature (i.e., ~20 ^{o}C or less). In C-1, the auxiliary heater is installed in the return air loop after water-to-air heat exchanger and before the desiccant wheel to maintain the return air temperature at the required regeneration temperature as shown in Fig. 1. A thermostat is used for the purpose of monitoring the outlet temperature of the air leaving the water to the air heat exchanger and accordingly, it switches on the auxiliary heater to increase the temperature of the air to the desired set temperature. In C-2, the auxiliary boiler is placed in the solar water heating loop to heat up the water before it enters into the water to air heat exchanger, as illustrated in Fig. 2. The temperature for the hot water leaving the auxiliary boiler is required to be determined which would serve to achieve the desired regeneration temperature of the air in the water to air heat exchanger.

C-3 scheme, as depicted in Fig. 3, is quite similar to the C-2 with the difference that no direct/indirect evaporative coolers are used in the process and return air loop and all of the cooling demand is achieved by a vapor-compression chiller (VCC).

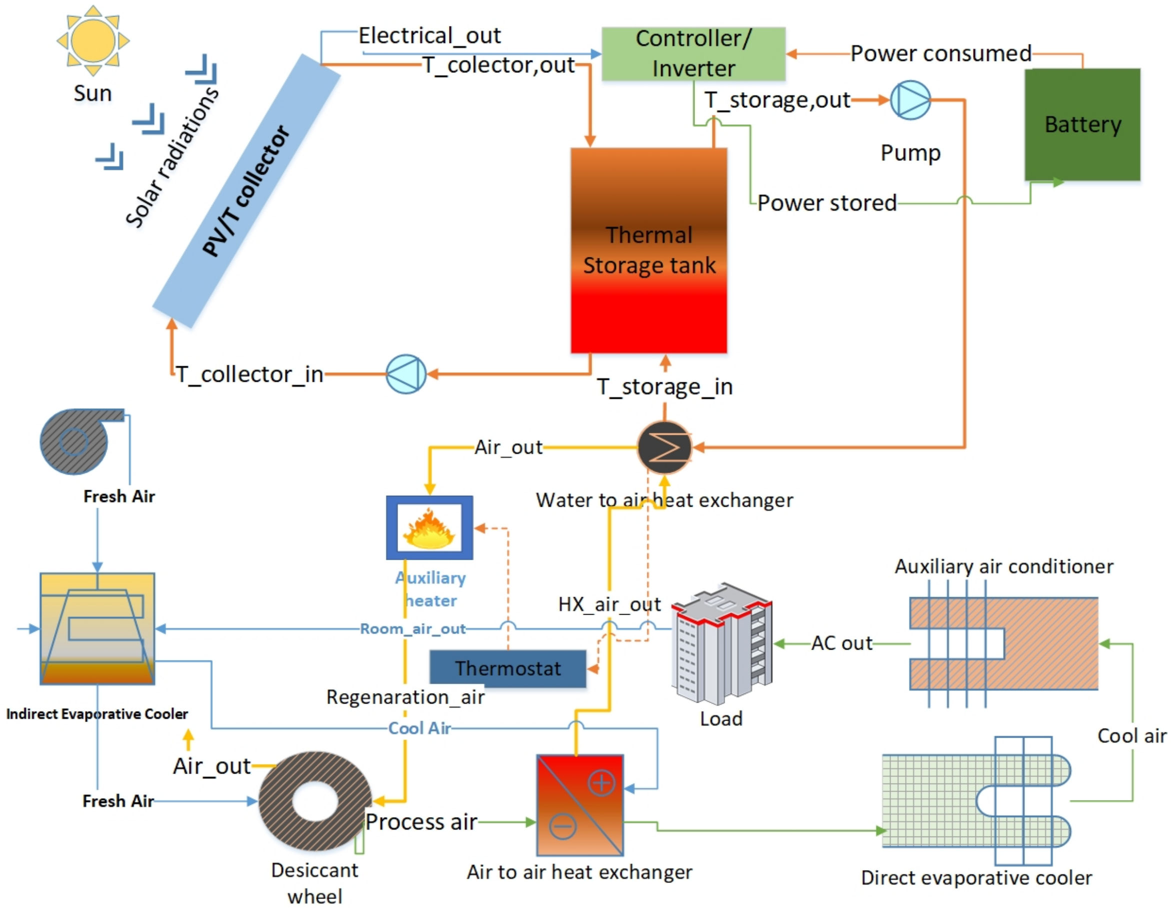

Fig 1: Schematic Diagram for C-1 scheme

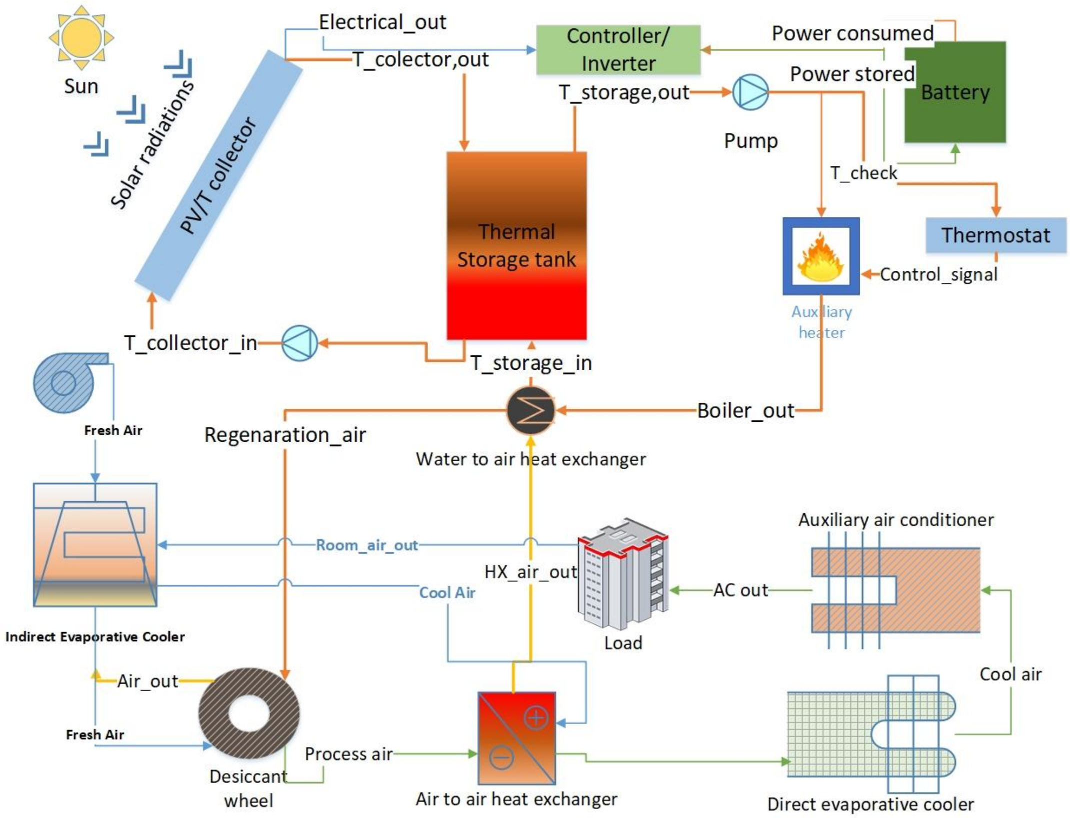

Fig 2: Schematic Diagram for C-2 scheme

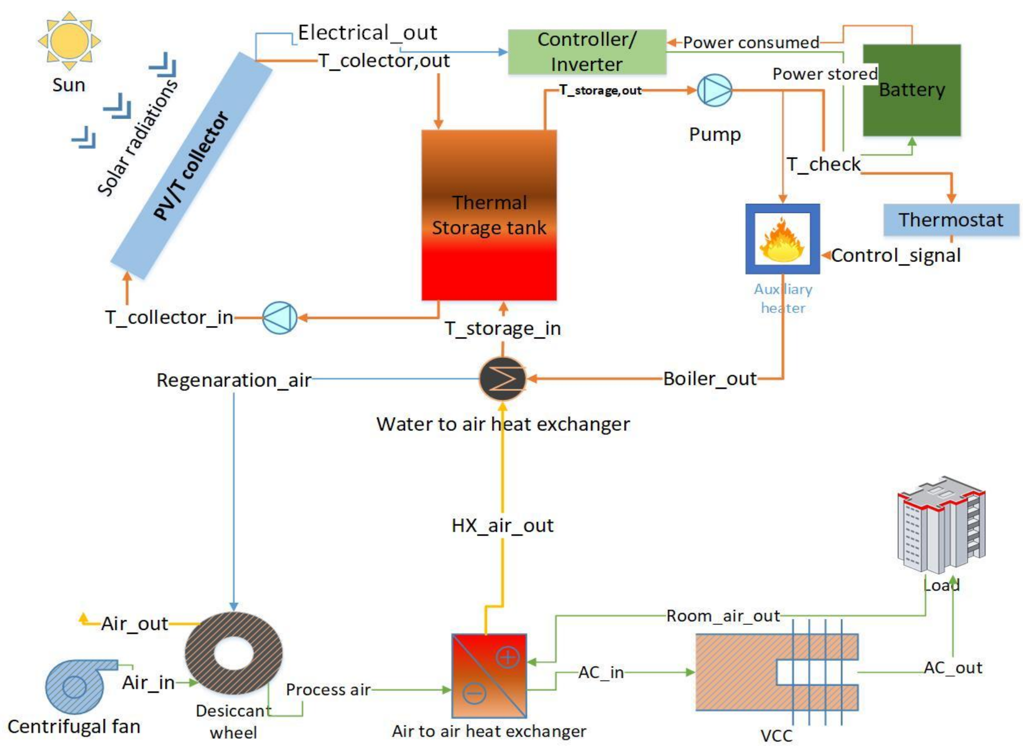

Fig 3: Schematic Diagram for C-3 scheme

3. TRNSYS Modeling

The system configurations of the solar-assisted desiccant-based air-conditioning system are modeled and simulated in TRNSYS (Version 18) for the climatic conditions of Lahore located in the Punjab province of Pakistan. TMY (typical meteorological year) file of weather data is used to simulate the weather parameters, such as available global solar radiation, ambient temperature, relative humidity, etc.

The weather data file for the location of Lahore (33.71° N, 73.06° E) in TRNSYS type-99 is used to simulate the climatic variables. Fig. 4 shows the hourly variation of available global solar radiation on the horizontal surface for the whole summer season (i.e., May-to-September). The hourly variation of ambient temperature and relative humidity is also depicted in Fig. 5 for the whole summer season. A prominent shift in the relative humidity from the month of June to July and onwards is quite evident in Fig. 5 and that is due to the annual regular rainy season in this region which usually lasts for about 2-3 months. The averaged relative humidity for the months of May and June is ~ 43 % while for the months July to Sep it is ~73 %.

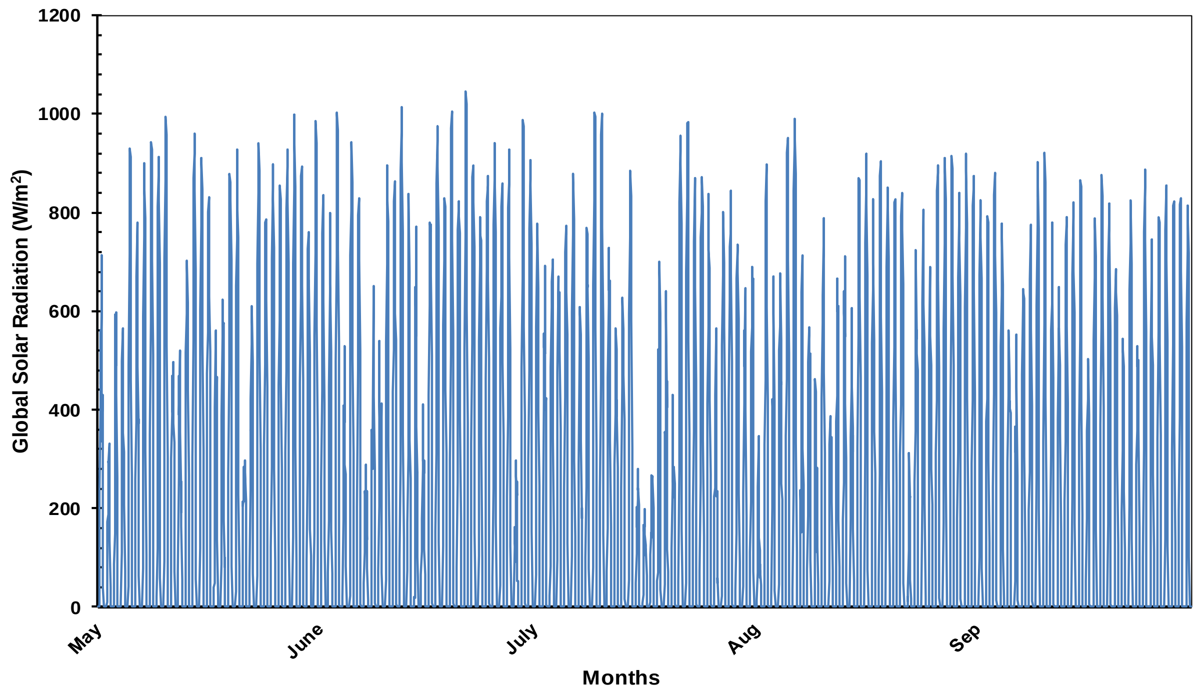

Fig 4: Hourly variation of available global solar radiation on a horizontal surface for the whole summer season

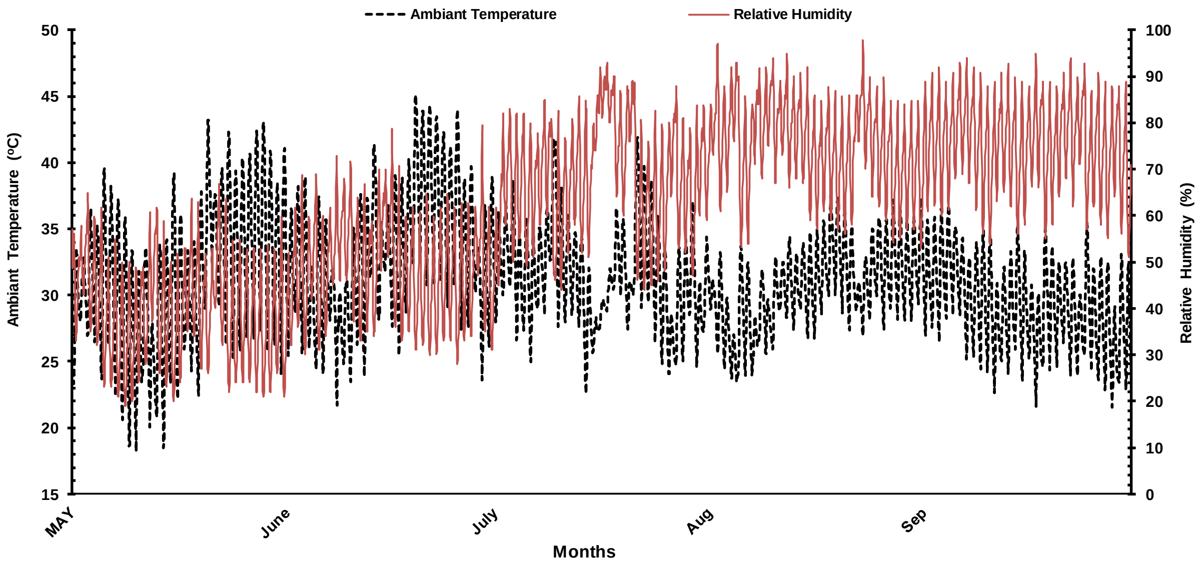

Fig 5: Hourly variation of ambient temperature and relative humidity over the whole summer season

Figs. 6-8 illustrate the pictorial views of the three configuration-schemes in the TRNSYS studio to analyze their thermal performance. Important assumptions of the developed models in the TRNSYS are as follows:

- Power losses during charging and discharging of battery and inverter are not considered.
- Energy losses from the connecting pipes, valves, etc. between various system components are neglected.
- Typical constant values of the thermophysical properties of air and water are used in the simulation.

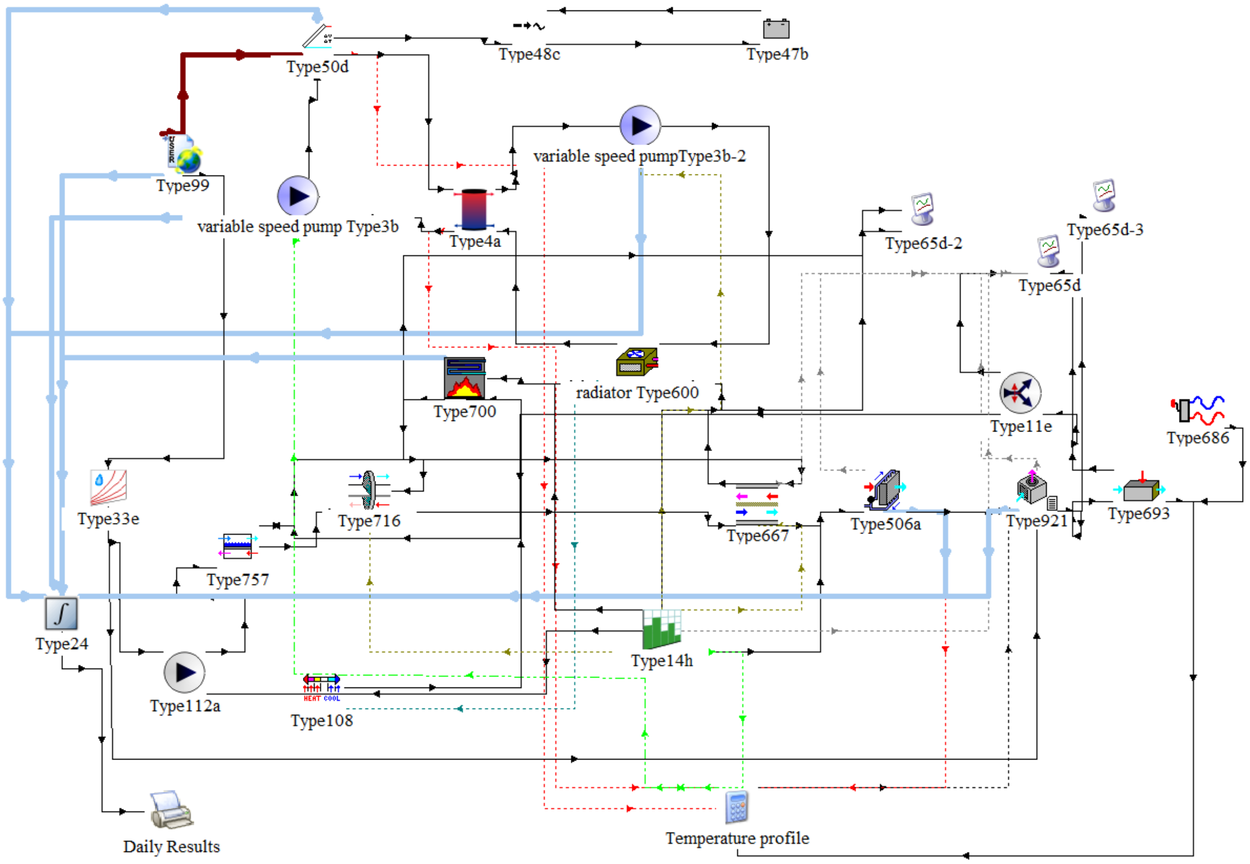

Fig 6: Pictorial view of C-1 in TRNSYS simulation studio environment

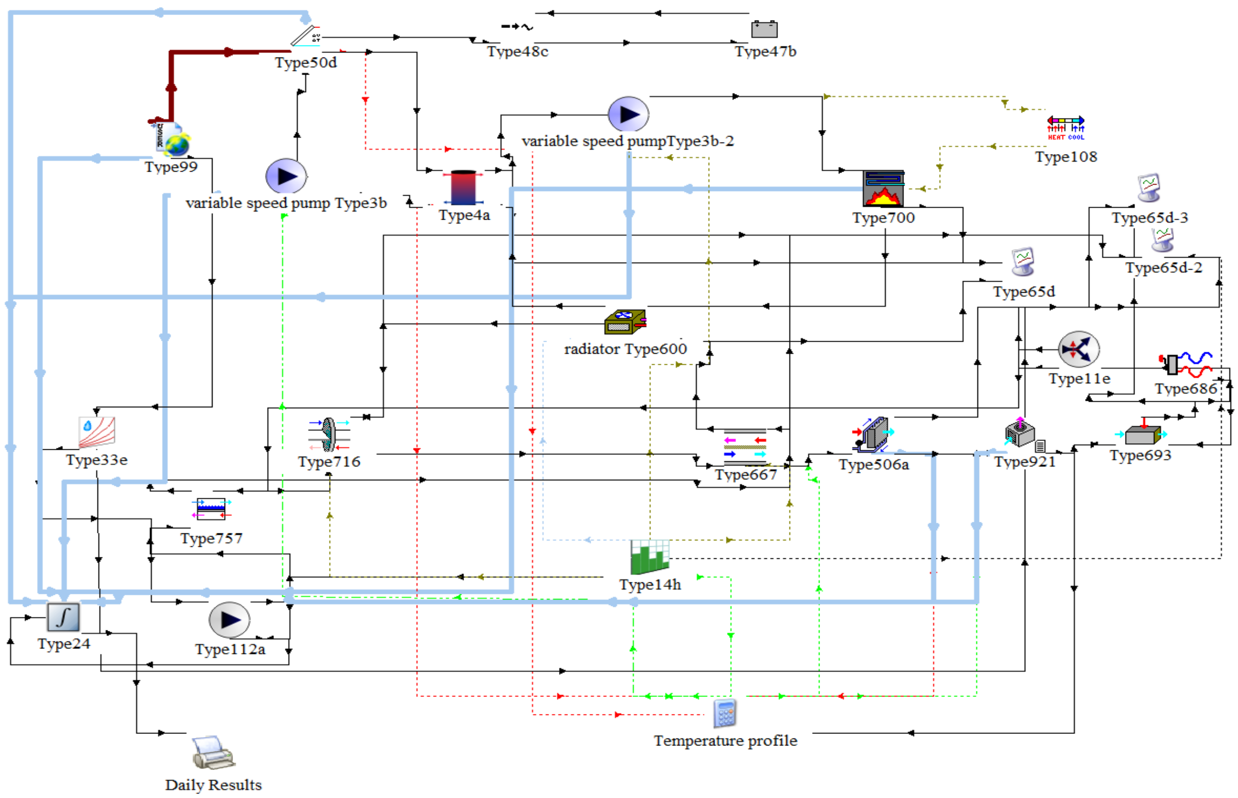

Fig 7: Pictorial view of C-2 in TRNSYS simulation studio environment

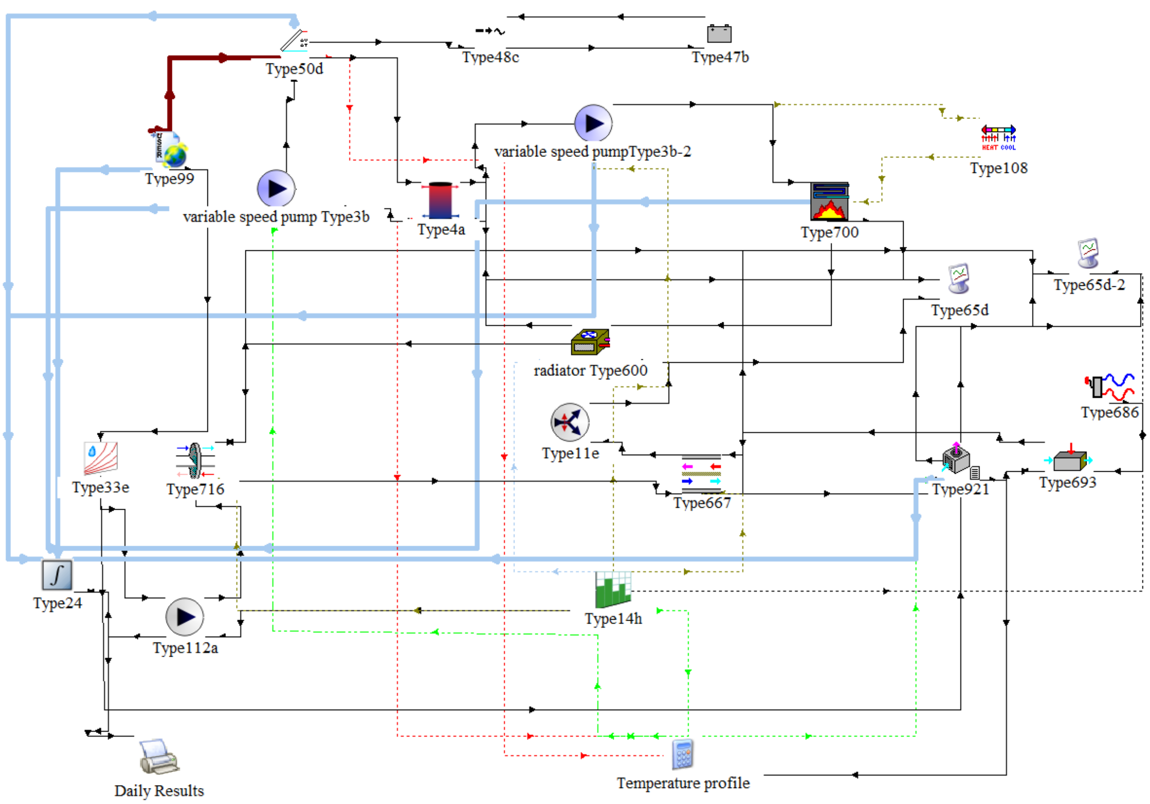

Fig 8: Pictorial view of C-3 in TRNSYS simulation studio environment

The PV/T Solar collector is the main energy source of the cooling system to regenerate the desiccant wheel and to power the auxiliary cooling source. The TRNSYS type-50 is used to model the operation of combined photovoltaic and flat plate thermal solar collector. The thermal energy gain (Q_u) of the PV-T collector is based on Hottel-Whillier equation and is given as:

$$Q_u = AF_R\{G(\tau\alpha) - U_L(T_i - T_a)\} \tag{1}$$

Where, A is the total collector area, G is the global solar irradiance on the tilted surface, $\tau\alpha$ is the effective transmittance-absorbtance product of the glazing and surface coating of the absorber plate, U_L is the overall heat loss coefficient from the collector to ambient and it corresponds to total heat loss of the solar collector due to difference between inlet fluid temperature (T_i) and ambient temperature (T_a). The overall heat loss coefficient (U_L) of the flat plate solar collector is approximated by Klein's equation [20]:

$$U_L = \frac{3.6}{\dfrac{N_G}{\dfrac{C}{T_p}\left[\dfrac{(T_f - T_a)}{N_G + f}\right]^{0.33} + \dfrac{1}{h_w}}} + \frac{3.6\sigma\left(T_f^2 + T_a^2\right)\left(T_f + T_a\right)}{\dfrac{1}{\varepsilon_p + 0.05N_G\left(1 - \varepsilon_p\right)} + \dfrac{2N_G + f - 1}{\varepsilon_g} - N_G} + U_{be} \tag{2}$$

Where;

$h_w = 5.7 + 3.8V_{air}\ (W/m^2K)$

$f = (1 - 0.04h_w + 0.0005h_w^2)(1 + 0.091N_G)$

$c = 365.9(1 - 0.00883\beta + 0.0001298\beta^2)$

Eq. (2) of U_L incorporates the effect of all the key design parameters, such as number of glass covers (N_G), mean fluid temperature (T_f), ambient temperature (T_a), mean absorber plate temperature (T_p), wind heat transfer coefficient (h_w), thermal emittance of plate and glass (ε_p, ε_g), collector tilt (β), and the combined heat loss coefficient from the bottom and edges of the PV-T collector (U_{be}). F_R in Eq. (1) is the collector flow factor which as a function of U_L, thermal capacitance of working fluid ($\dot{m}C_p$), collector efficiency factor (F'), and collector area (A) is defined as [20]:

$$F_R = \frac{\dot{m}C_p}{AU_L}\left\{1 - exp\left(\frac{F'U_LA}{\dot{m}C_p}\right)\right\} \tag{3}$$

The desiccant wheel is the essential component of any desiccant based cooling system.TRNSYS type 716 is a desiccant wheel which actually models a rotating solid silica gel based dehumidifier whose performance is computed on the basis of *F1-F2* potentials [21] [22]. The model uses an iterative scheme and based on entering air conditions of the fresh or process air and return air estimates the exit air conditions of the desiccant wheel on both process and return air sides. A brief description of all the main

TRNSYS components used in the modeling of systems along with their technical specifications are detailed and discussed in Table-1.

Table 1: Description of TRNSYS elements and design input parameters

Component	Type in TRNYS	Input Parameters	Description
PV-T Solar Collector	Type50d	• Collector efficiency factor (*F'*): 0.7 • Absorptance (α) and emittance of collector plate (ε): 0.9 • No. of glazing: 1 • Extinction Coefficient and glazing thickness: 0.03 • Heat loss coefficient of the thermal collector: 5.5 W/m^2.K • PV cell area to absorber area: 0.5 • Efficiency of the PV cell at the reference temperature (20 ^{o}C): 0.2	It is a flat plate PV-T solar collector, which simulates the operation of the thermal and electrical output of the collector under a given set of input parameters.
Storage Tank	Type4a	• No. of nodes: 10 • Tank heat loss coefficient: 0.833 W/m^2 K	It is a stratified storage tank without a heat exchanger and water as the heat storage medium. The fluid flow from the tank towards collectors always leaves from the bottom node and flow towards load always leaves from the top node.
Pump	Type3b	--	The pumps are used to maintain the desired flow rate of the working fluid in various loops of the system. The optimum flow rate in solar heating loops is estimated as discussed in Section-5.1.
Radiator	Type 600	• Coil bypass fraction: 0.1 • Air side flow rate (cold): 1200 kg/hr • Water side flow rate (hot): 350 kg/hr.	This component model a 2-pipe fan coil model; delivering heat and/or cold to the air stream from a source liquid stream, which in the present case is the hot water from the solar loop.

Auxiliary Boiler	Type 700	• Boiler efficiency: 0.78 • Combustion efficiency: 0.85	This component is a steam boiler, which adds heat energy to the working fluid to raise its temperature to the desired value (if required). In C-1, it is used to heat the air while in C-2 and C-3 it heats the water to a certain desired temperature.
Storage Battery	Type 47b	• Cell energy capacity: 16.7 Ah • Charging efficiency: 0.9	It is lead-acid storage battery operates in conjunction with solar cell array and power conditioning components. It utilizes formulas relating to battery voltage, current, and the state of Charge.
Inverter/Regulator	Type 48c	• Regulator Efficiency: 0.78 • Inverter Efficiency: 0.96	It is a combination of inverter and regulator. In PV systems, regulator distributes DC power from the solar cell array to and from a battery. If the battery is fully charged or needs only a taper charge, excess power is either dumped or not collected by turning off parts of the array. While inverter is used to convert the DC power to AC and sends it to the load.
Desiccant Wheel	Type 716	• Humidity mode: based on relative humidity which is linked to the weather data file. • Regeneration air temperature: varied from 50-70 ^{o}C (see details in Section 5.3). • Process air flow rate: 2000 kg/hr • Regeneration air flow rate: 1200 kg/hr	This element simulates the operation of rotary desiccant dehumidifier containing silica gel as the desiccant material. Its performance is based on equations developed by Jurinak [21]. Psychometric conditions of the entering process and return air are used as the input parameters.
Air-to-Air Heat Recovery Device	Type 667	• Effectiveness of heat exchanger: 0.6 • Process air flow rate: 2000 kg/hr • Return air flow rate: 1200 kg/hr	The type-667 models the operation of an air-to-air sensible heat exchanger based on constant effectiveness (ε)-minimum capacitance approach. The amount of heat exchange is [23]: $\dot{Q}_{sens} = \varepsilon_{sens} C_{min} (T_{return,in} - T_{process,in})$
Direct Evaporative Cooler (DEC)	Type 506a	• Humidity mode: based on relative humidity.	The component models the direct evaporative cooler to compute the outlet air conditions

		• Saturation efficiency: 0.8	based on inlet air conditions and saturation efficiency. The model assumes constant wet-bulb temperature of the air from the entrance to exit. The minimum temperature of the air leaving the device is given as [23]: $T_{air,o} = T_{air,i} - \eta_{sat}\, T_{wbd}$
Indirect Evaporative Cooler (IDEC)	Type 757	• Humidity mode: based on relative humidity.	IDEC is used in C-1 and C-2 to sensibly cool the process air before entering the desiccant wheel. Type-757 is a TRNSYS element which computes process air outlt temperature (dry-bulb) by assuming a constant value of wet-bulb temperature of the secondary (i.e., return air) coming from the building.
Vapor Compression Chiller	Type 921	• Rated cooling power: 2.5 TR • Evaporator air flow rate: 7200 kg/hr	It is a unitary air conditioning unit for commercial or residential use. In the present case, the model calculates the cooling capacity and power consumed on the basis of entering air properties and the specified flow rate of the air coming from DEC. The unit is programmed to maintain the continuous air supply between 15^{o}C to 20^{o}C during the working hours.
Cooling Load	Type 682	• Imposed cooling load on the fluid stream: 2.5 TR	This component allows the user to impose a fixed value of cooling or heating load on the working fluid coming from the air conditioning unit (type 921). The building loads are added to or subtracted from that liquid, resulting in an outlet temperature just past the interaction point.
Cooling Load Variation	Type 686	• Peak cooling load: 2.5 TR • Start of the cooling season: 2160 hr. • End of cooling season: 6552 hr. • Peak cooling load hour: 3756 hr.	It generates hourly cooling and heating loads for a synthetic building based on defined peak cooling/heating loads (see Fig. 7)

Forcing Function	Type 14h	--	This type is used to force the system to operate for a certain time-interval during the 24-hour period of the day. In the current study, the system is made to operate daily from 0900-1700 hrs. for the whole summer season, except on weekends.
Thermostat	Type 108	--	This is a five-stage room thermostat which is used to control the outlet temperature of the fluid leaving the auxiliary boiler. In C-2 and C-3, it monitors the outlet temperature of the water leaving the solar collector and send the signal to the auxiliary boiler (Type 700) to switch on if the temperature is below a certain selected value. In C-1, it is used to monitor the outlet air temperature of the air leaving the water to air heat exchanger (see Fig. 1)

As described in Table-1, type-682 and 686 are employed to model the cooling load and its variation over the whole summer season. The hourly variation of the cooling demand is shown in Fig. 9.

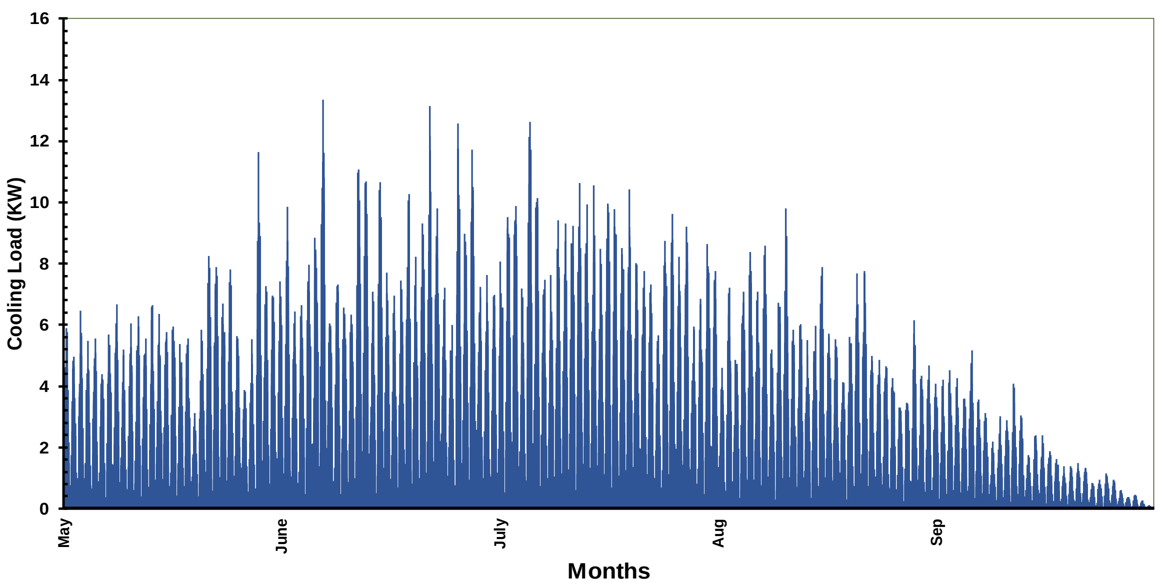

Fig 9: Cooling load profile for the whole summer season

4. Performance Parameters

As the main focus of the examined system configurations is on the optimization of thermal and electrical energy generation loop from solar and/or auxiliary energy source, the performance evaluation criterion is based on solar energy-related performance factors. The thermal performance of the solar PV/T collector is evaluated based on the thermal efficiency of the collector and it is defined as the ratio of the useful thermal energy produced from the PV/T collector to the available global solar irradiance on the collector area. It is mathematically given as:

$$\eta_{th}=\frac{Q_s}{GA} \tag{4}$$

Where; Q_s is the rate of useful energy gain of solar collector, G is the global solar irradiance on the tilted surface, and A is the solar collector area.

Solar fraction (SF) is an important performance criterion which represents the fraction of the total required energy to drive a cooling system which is fulfilled by the solar energy. In the present study, the thermal and electrical solar fraction of the considered systems are defined as [24]:

$$SF_{th} = \frac{Q_s}{Q_s + Q_b} \tag{5}$$

$$SF_{elec} = \frac{P_s}{P_s + P_{aux}} \tag{6}$$

Where; Q_s and P_s , respectively, are the useful thermal and electrical energy gain of the PV/T solar collector, Q_b is the thermal energy contribution of the auxiliary boiler, and P_{aux} represents the electrical power consumption of all the auxiliary electrical appliances, i.e., pumps, fan, evaporative cooler, and vapor compression chiller.

The primary purpose of any solar-based heating and/or cooling system is to save energy in comparison to an equivalent system running on the conventional or non-solar energy source. This saving in energy can be quantified by defining it in a mathematical expression and termed as primary energy savings [25]. A modified form of primary energy savings used in the current study is given as:

$$f_{sav} = 1 - \left[\frac{\dfrac{Q_b}{\varepsilon_f \eta_b} + \dfrac{E_{el}}{\varepsilon_{el}} + \dfrac{\dfrac{Q_{c,ac}}{COP_{ac}} - P_s}{\varepsilon_{el}}}{\dfrac{Q_{c,ac-ref}}{COP_{ac}\varepsilon_{el}}}\right] \tag{7}$$

Where Q_b, E_{el}, and $Q_{c,ac}$, respectively, represent the thermal energy consumed by the auxiliary boiler (type-700), electrical energy consumptions of all the major electrical appliances (pumps, fans/blowers, desiccant wheel etc.), and cooling energy produced by the conventional air conditioning unit (type-921) in the solar-based desiccant cooling systems. The term ε_{elec} is the efficiency of the thermal power plant and its typical value is taken as 0.4. COP_{ac} is the coefficient of performance of an air conditioner and a value of 2.8 is assumed for the common vapor compression chiller. The conversion efficiency of the fossil fuel (ε_f) and the thermal efficiency of the auxiliary boiler (η_b) in Eq. (7) are taken as 0.9 and 0.95, respectively. $Q_{c\text{-}ac\text{-}ref}$ is the total primary energy required to run a conventional vapor compression-based air conditioning unit to meet the same cooling load as by the solar-based cooling systems.

5. Results and Discussion

Results are presented here based on dynamic simulations of the three system configuration schemes which were performed in TRNSYS 18.0 for the whole summer period typically ranging from May to September. The influence of various design parameters is studied and discussed in this section based on seasonal, monthly, and daily simulations.

5.1 PV/T Solar Collector Tilt and Flow Rate

Thermal solar fraction for all system configurations is estimated as a function of varying collector tilt as illustrated in Fig. 10. It can be seen that for all cases both thermal and electrical *SF* increases slightly with the increase in collector tilt from 0-15^o and then drops with increasing tilt angle beyond 15^o.

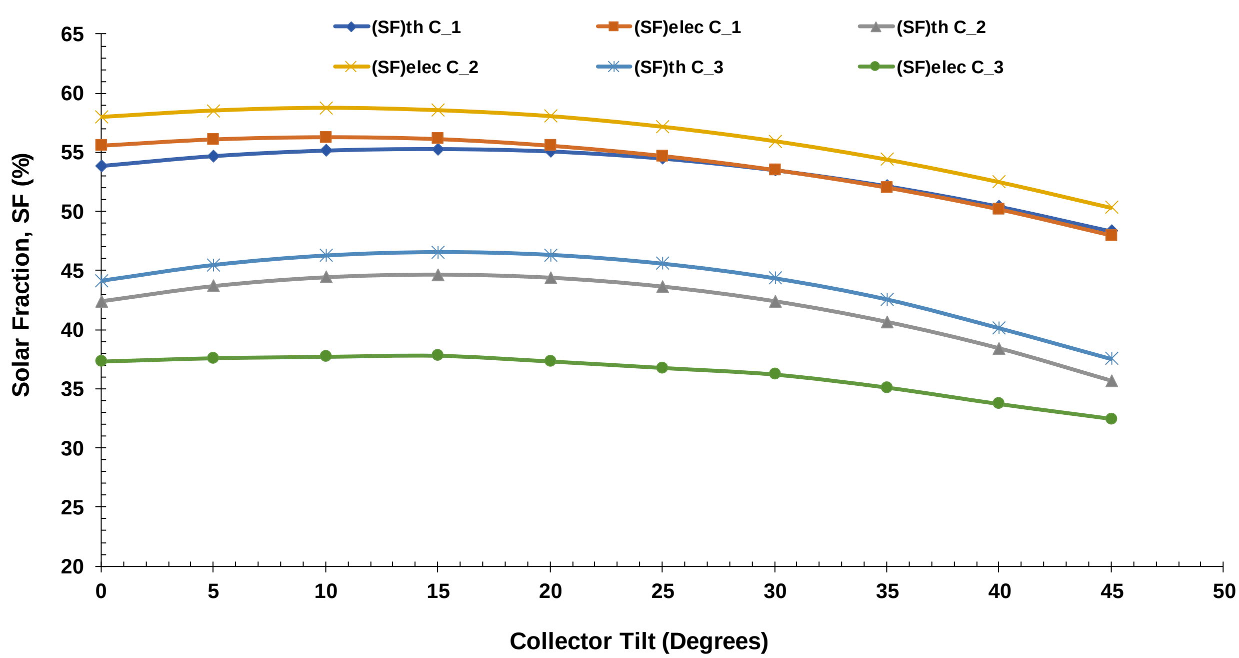

Fig 10: PV/T Collector Tilt versus Solar Fraction (For A_c = 25 m^2, T_{reg} = 60 ^{o}C, $\dot{m}_{col}$ = 400 kg/hr)

The optimum tilt (β) of the flat plate type solar collector for a certain location (i.e. latitude, φ) on any summer day (i.e. positive declination angle, δ) can be mathematically estimated as [26]:

$$\beta = \varphi - \delta \tag{21}$$

Eq. (21) is used to compute the optimum collector tilt for the current location of Lahore (φ = 31.52^o N) and for the average day of each month of the whole summer season. The estimated averaged value for the whole summer season is ∼15^o which is the same as the optimum values computed through TRNSYS simulation models. This matching of simulation and analytical results also serves the purpose of the validation of the TRNSYS models.

The performance of any solar thermal collector is a strong function of working fluid's flow rate (Eq. (3)). Fig. 11 depicts the variation of the useful energy gain of the PV/T collector with respect to the fluid flow rate for all three configurations. It is observed that heat gain of the PV/T solar collector in all configurations significantly increases with the rise in flow rate from 50-300 kg/hr and then stabilizes as the increase is quite mild after this. A flow rate of 400 kg/hr is, therefore, referred to as an optimum flow rate for PV/T solar collector to be used in all configuration schemes.

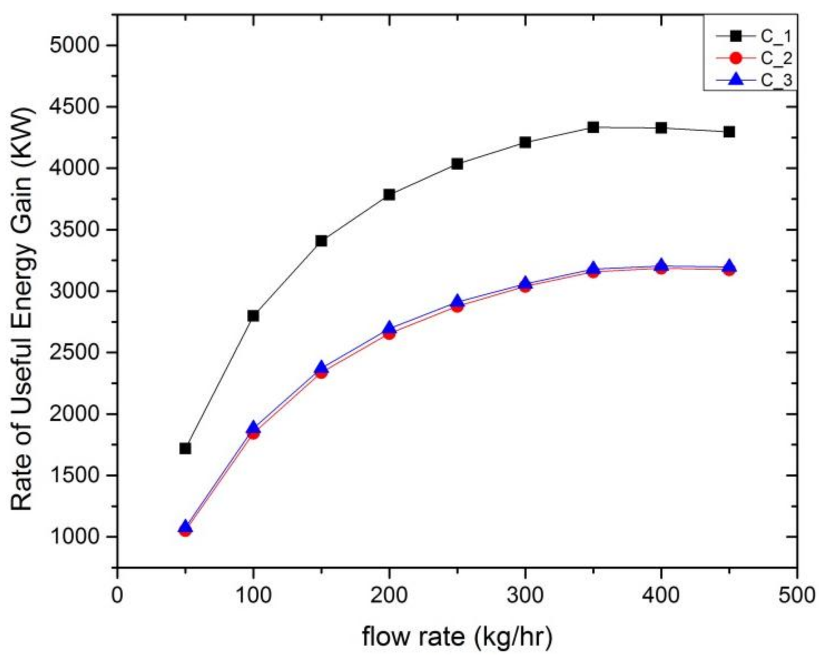

Fig 11: Graph between solar collector flow rate versus collector heat gain (for A_c = 25 m^2, $\beta = 15^o$, T_{reg} = 60 ^{o}C)

5.2 Volume of Storage Tank

The effect of storage tank size is studied by plotting the variation of SF_{th} with respect to storage volume for all configuration schemes and for three different PV/T collector areas, as illustrated in Fig. 12. For all collector areas and for all system configurations the trend of curves shows a rise in SF_{th} with the increase in storage volume to a certain point and then decreases. The peak value of SF in each case corresponds to the optimum value of storage size for a certain configuration scheme and for a particular solar collector area. It is also observed that for each configuration the optimum value of the storage tank increases with the increase in the solar collector areas.

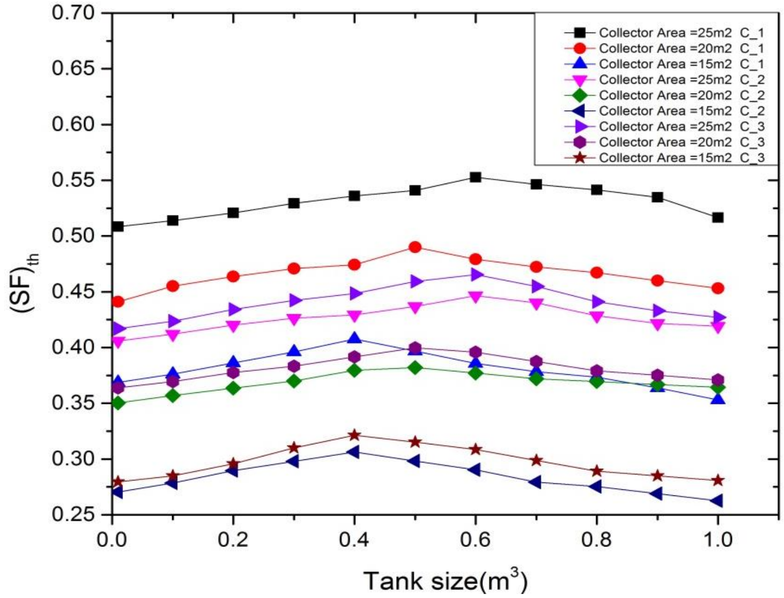

Fig 12: Variation of Therma Solar Fraction SF_{th} with tank size (for A_c = 25 m^2, β = 15^o, T_{reg} = 60 ^{o}C)

5.3 Regeneration Temperature

The influence of regeneration temperature of the regeneration air entering the desiccant wheel on the thermal solar fraction (SF_{th}) and primary energy savings (f_{sav}) is estimated as depicted in Figs. 13 and 14 for all configurations schemes with the same collector area of 25 m^2. The results demonstrate the fact that SF_{th} and f_{sav} are very sensitive to regeneration temperature (T_{reg}), as increasing T_{reg} significantly increases the dependency on the auxiliary boiler. Figs. 13 and 14 show that f_{sav} decreases by ~ 90 % while SF_{th} decreases by ~50 % with the increase in regeneration temperature from 50 to 70 ^{o}C. It is evident that the collector area must be increased to operate the desiccant wheel at higher temperatures and to achieve reasonable values of SF_{th} and f_{sav}.

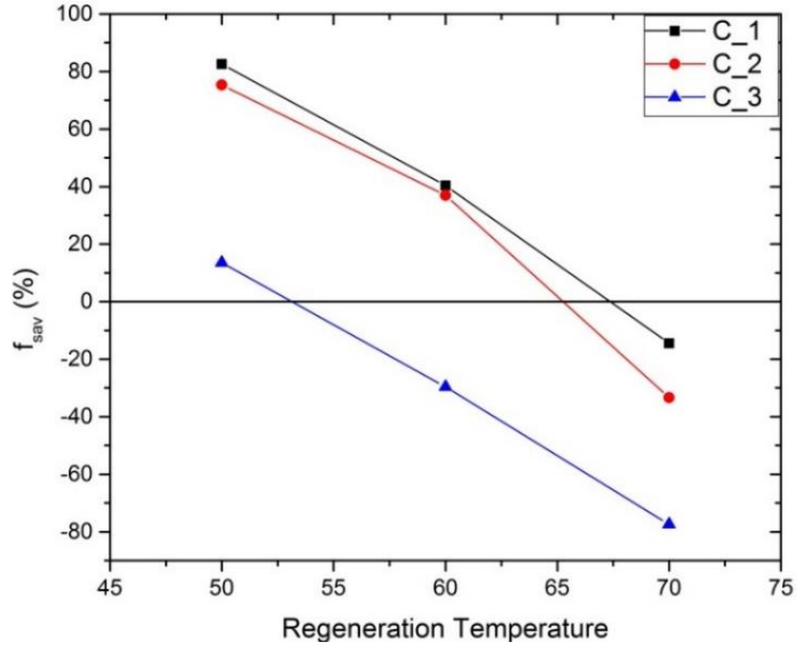

Fig 13: f_{sav} versus Regeneration Temperature (For A_c = 25 m^2, β = 15^o, $\dot{m}_{col}$ = 400 kg/hr)

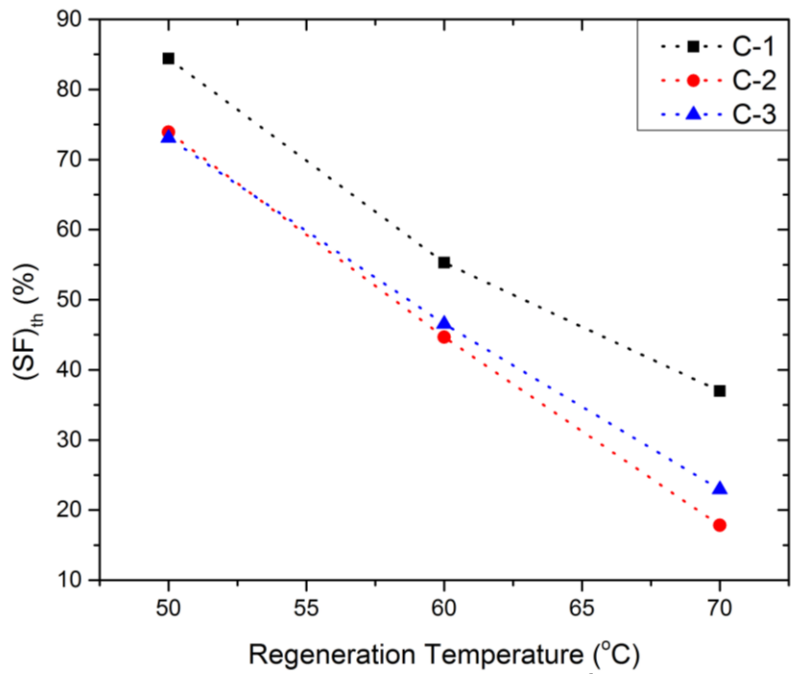

Fig 14: SF_{th} versus Regeneration Temperature (For A_c = 25 m^2, β = 15^o, $\dot{m}_{col}$ = 400 kg/hr)

5.4 Size of PV/T Solar Collector

Figs. 15 and 16 show the estimated values of seasonal primary energy savings (f_{sav}) thermal solar fraction (SF_{th}), respectively, as a function of PV/T collector area. Both f_{sav} and SF_{th}, obviously, increase with the increase in collector area for all system configurations. Fig. 15 shows that C-1 give rise to highest f_{sav} and for C-3 it is worst as it remains negative for collector area up to 35 m^2. Similarly, it can be seen in Fig. 16 that C-1 also results in highest SF_{th} while the difference between C-2 and C-2 is marginal but values of SF_{th} are well above zero for all cases. In C-2 and C-3, the auxiliary heater is installed in the solar water heating loop to heat the water to a much higher temperature (~ 68-70 ^oC) to heat the return air in the water-air heat exchanger to the required regeneration temperature (e.g. for 60 ^oC). Also, due to the higher specific heat of the water than air, the auxiliary heater requirement is much larger in C-2 and C-3 than in C-1where auxiliary heater is installed in the return air loop of the desiccant cooling system to directly heat the return air to the desired regeneration temperature of ~60 ^oC. The graph of SF_{elec} in Fig. 17, however, indicates a marginal difference between C-1 and C-2 while C-3 results in significantly lower values of SF_{elec}. This is due to the fact that in C-3 no direct or indirect evaporative cooler is utilized and all the cooling requirement is furnished by the auxiliary cooling system and that also resulted in negative values of f_{sav} in Fig. 15. Overall, it can be concluded that a collector area of at least 30 m^2 is required to achieve 50 % f_{sav} for C-1 and C-2 while C-3 without the evaporative cooler is not a feasible preference for a solar-based desiccant cooling system.

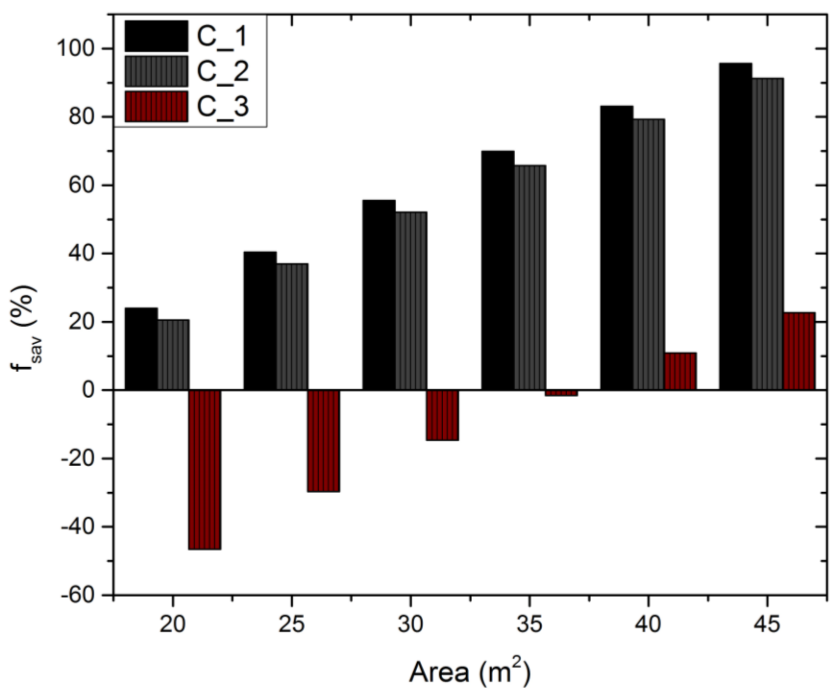

Fig 15: Graph between f_{sav} and Collector Area (for β = 15^o, T_{reg} = 60 ^oC, $\dot{m}_{col}$ = 400 kg/hr)

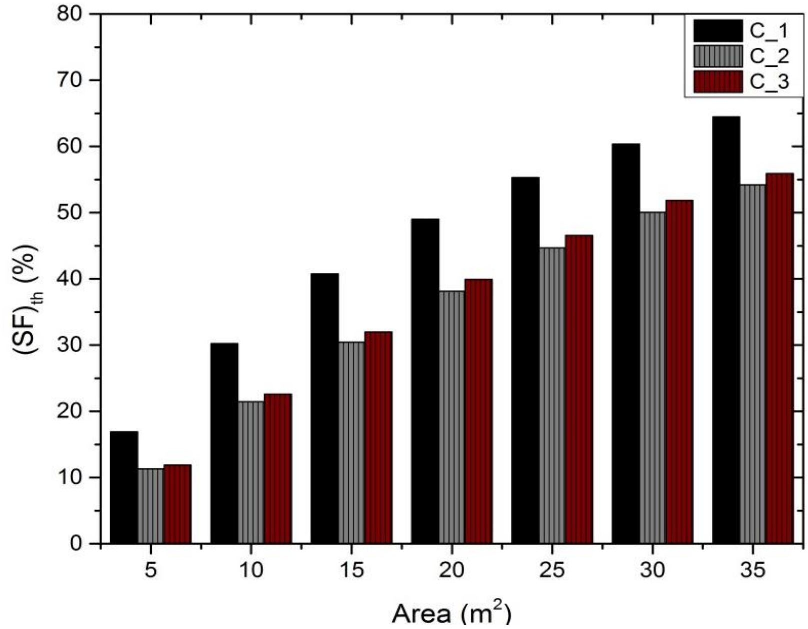

Fig 16: Graph between SF_{th} and Collector Area (for β = 15^{o}, T_{reg} = 60 ^{o}C, $\dot{m}_{col}$ = 400 kg/hr)

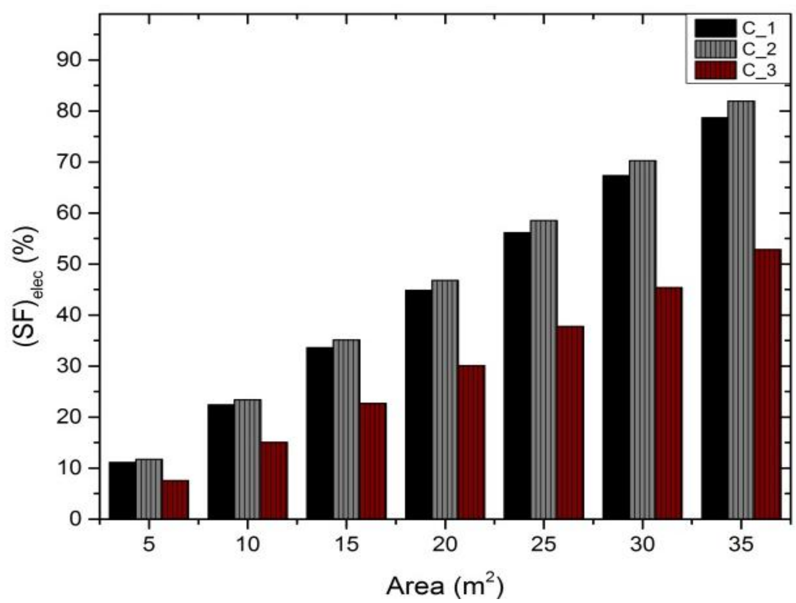

Fig 17: Graph between SF_{elec} and Collector Area (for β = 15^{o}, T_{reg} = 60 ^{o}C, $\dot{m}_{col}$ = 400 kg/hr)

The thermal efficiency of the PV/T solar collector is shown for three configuration schemes as a function of the collector area in Fig. 18. The thermal efficiency of the PV/T collector (η_{th}) is substantially larger for C-1 than C-2 and C-3 under the same ambient conditions. It is owing to the higher collector's fluid temperature in C-2 and C-3 than in C-1 as illustrated in Figs. 21-23 (section 5.5) where temperatures and energy variations across PV/T solar collector are plotted for a typical summer day. As the increase in solar collector area also prompts a higher collector temperature which corresponds to rise in the overall heat loss from the solar collector to the cold ambient and thus decrease in collector's thermal efficiency (η_{th}) with the rise in collector area is observed in Fig. 17. This decrease in η_{th} is more prominent in C-1 (i.e. up to 10 %) than in C-2 and C-3 (i.e. up to 5 %) with the rise in collector area from 5-35 m^2.

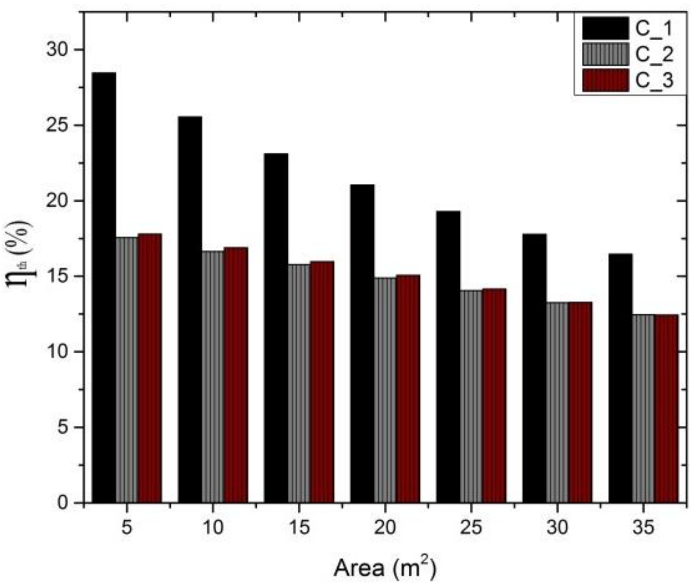

Fig 18: Thermal Efficiency VS AREA (for β = 15°, T_{reg} = 60 °C, $\dot{m}_{col}$ = 400 kg/hr)

5.5 Monthly Performance Indicators

Simulation results based on monthly basis are also compiled and presented in the form of f_{sav} and SF_{th} as shown in Figs. 19 and 20, respectively. The overall trend shows that the values of f_{sav} and SF_{th} drops in the months of July and August in comparison to May and June. It is due to the humidity values of the ambient air which is significantly higher during the months of July-September than in May and June (see Fig. 5). The effect of increasing humidity of the process air is that its temperature also rises after it passes through the desiccant wheel [27] and this ultimately results in increased primary energy demand of the auxiliary boiler and/or of the auxiliary air conditioner. The month of September is an exception as the required cooling demand is lowest in this month.

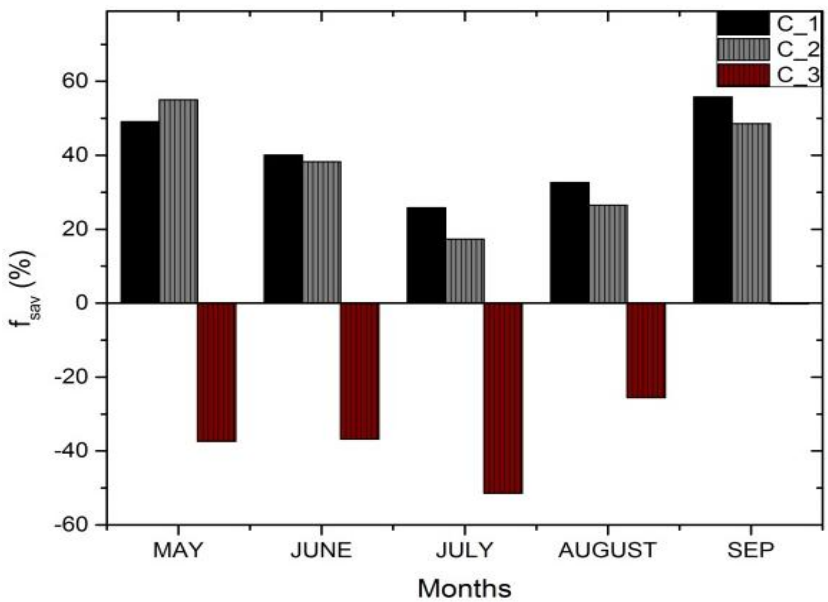

Fig 19: Primary energy savings based on monthly simulation (for β = 15^o, T_{reg} = 60 ^{o}C, $\dot{m}_{col}$ = 400 kg/hr)

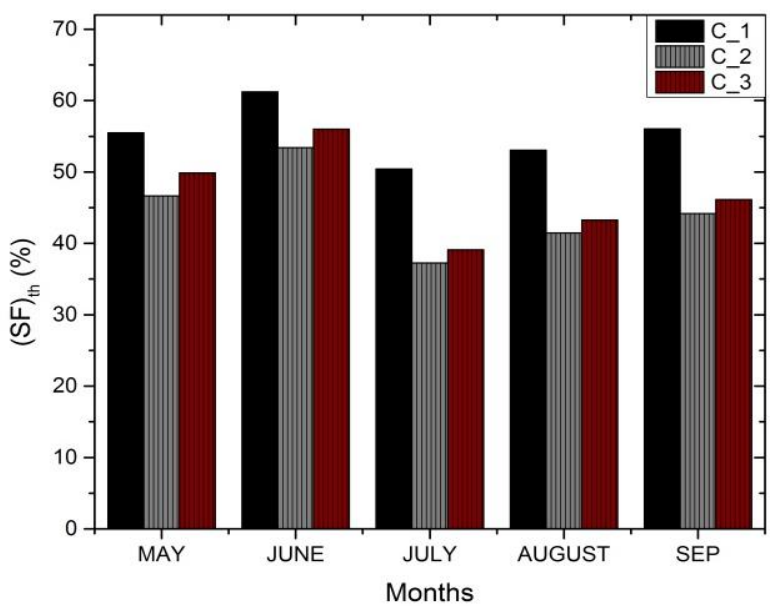

Fig 20: Primary energy savings based on monthly simulation (for β = 15^o, T_{reg} = 60 ^{o}C, $\dot{m}_{col}$ = 400 kg/hr)

5.5 Typical Day Profiles

The temperature and energy flow profiles of a typical day enable to interpret and understand the operation of the whole system and its individual components in a particular configuration scheme which resulted in various trends as seen in Sections 5.1 to 5.4. In this section the variation of key dynamic parameters, i.e., temperatures (T_{col_in}, T_{col_out}, T_{aux_in}, T_{aux_out}, T_{reg}, T_{anb}, T_{dec_out}, T_{evap_out}, T_{aaHX_out}, T_{vcc_out}) and energy flows (Q_u, P_{evap}, P_{col}, G, Q_{aux}, P_{vcc}) across different system components of the system in all three system configurations are depicted for a typical summer day (July 2) in Figs. 21-26.

Figs. 21-23 show that the daily mean fluid temperature of the supply air entering the room (T_{vcc_out}) to fulfill the cooling demand is in the range of ∼18 ^{o}C for all the configuration schemes. It can be observed that the temperature of the fluid leaving the auxiliary boiler in C-2 and C-3 are significantly higher (∼68 ^{o}C) than in C-1 (∼60 ^{o}C). This ultimately makes the entire solar loop and PV/T collector in C-2 and C-3 operate at higher fluid temperature. Mean fluid temperature in the PV/T collector ($T_{col,av}$) in C-1 is ∼53 ^{o}C while in C-2 and C-3 it is in the rage of 56-58 ^{o}C. This makes the useful energy gain of the PV/T collector (Q_u) smaller in C-2 and C-3 (∼2.2 kW) than in C-1 (∼3.4 kW), illustrated in energy profiles in Figs. 22-24. This resulted in the lower thermal efficiency of the PV/T collector in C-2 and C-3 than in C-1 (Fig. 18) which leads to a higher contribution of the heat energy from the auxiliary boiler (Q_{aux}) in C-2 and C-3 and hence lower SF_{th} than in C-1 (See Figs. 24-26).

Energy profiles of all configuration schemes also demonstrate that energy consumption of the auxiliary cooling system (P_{vcc}) is highest for C-3, (i.e., ∼3.33 kW) compared to ∼ 1.5 kW for C-1 and C-2, and therefore it resulted in lowest SF_{elec} and f_{sav} amongst all the configurations. The absence of evaporative coolers in C-3 eventuated a higher daily mean temperature of the supply air leaving the air-to-air heat exchanger or entering the auxiliary cooler (i.e., ∼39 ^{o}C) as opposed to ∼27 ^{o}C in C-1 and C-2. This concludes the fact that the absence of evaporative coolers is not at all a viable option for the demonstrated solar-based desiccant cooling systems at least for the current location of Lahore (31.52° N, 74.36° E).

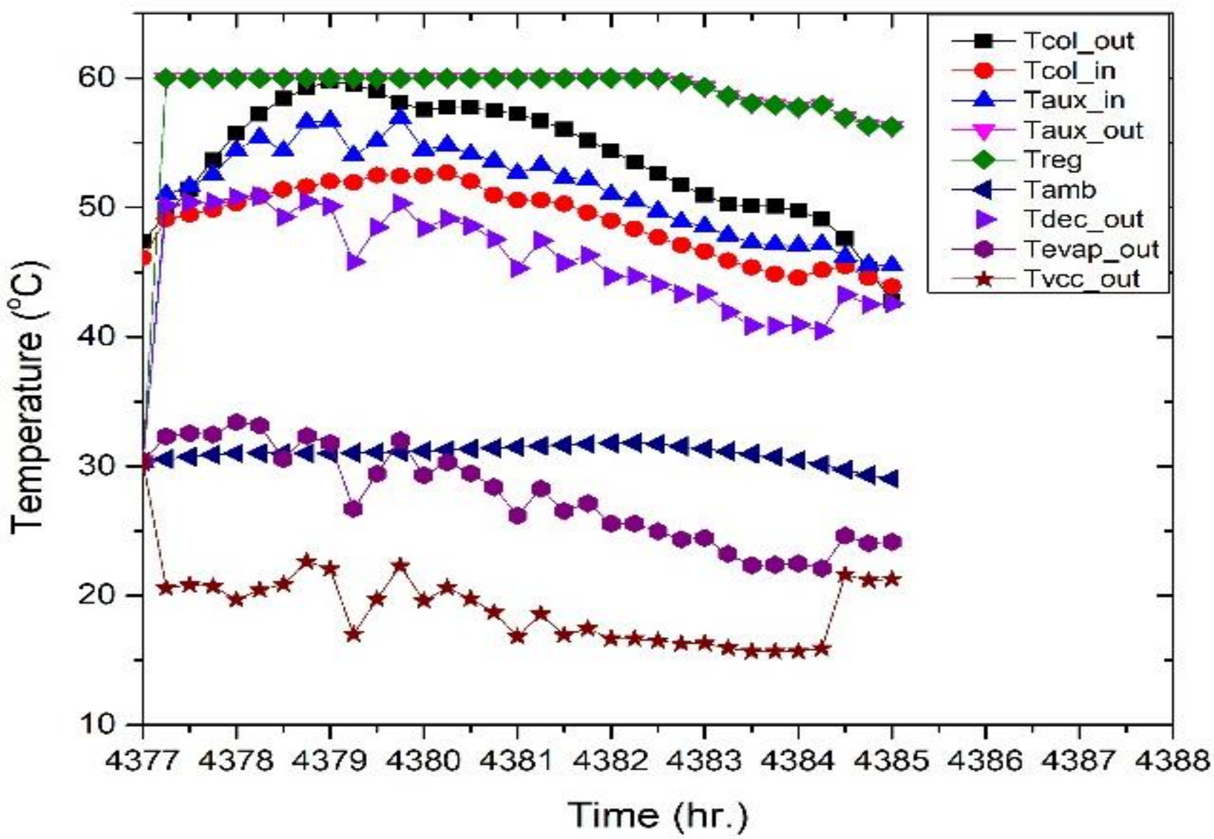

Fig 21: Temperature Profile for a Single Day C-1 (for β = 15^{o}, $T_{reg} \approx$ 60 ^{o}C, $\dot{m}_{col}$ = 400 kg/hr)

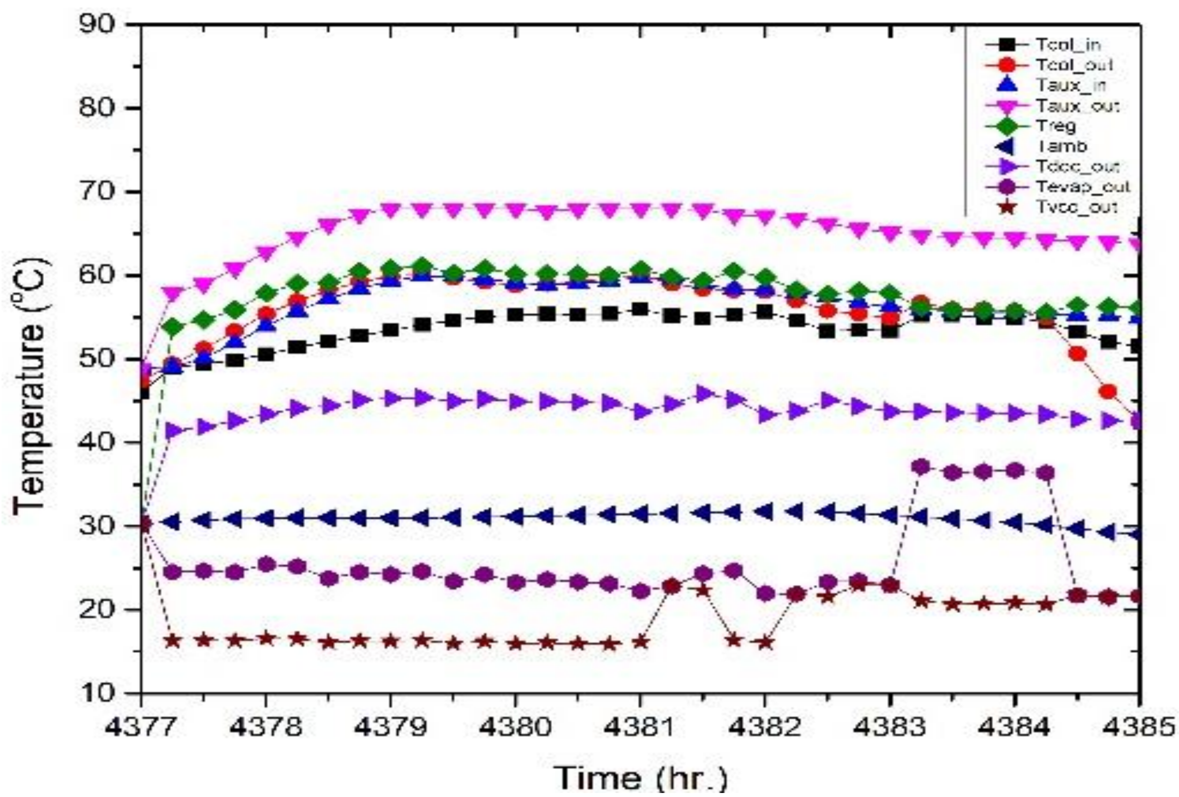

Fig 22: Temperature Profile for a Single Day C-2

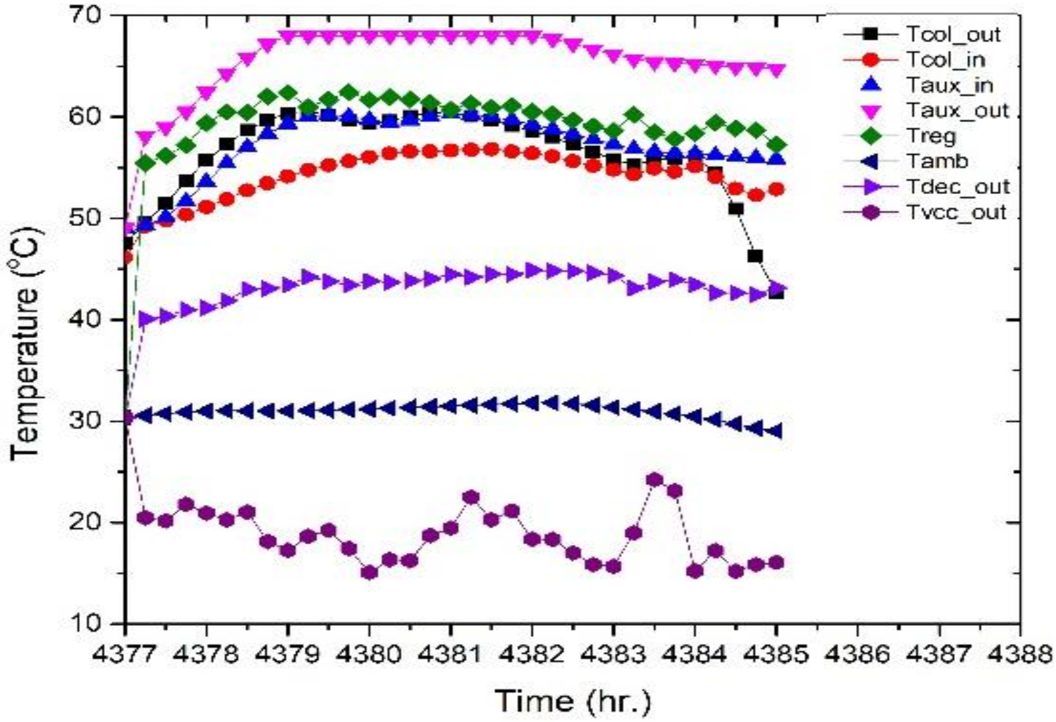

Fig 23: Temperature Profile for a Single Day C-3

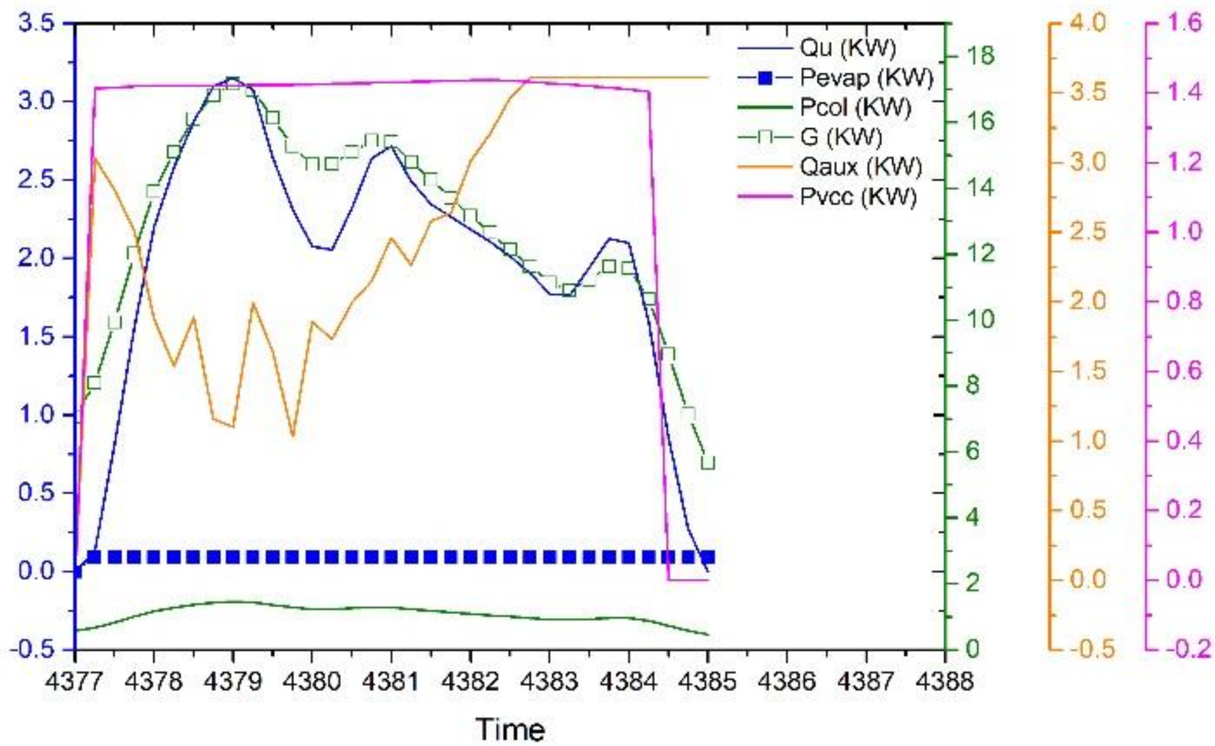

Fig 24: Energy Profile for a Single Day C-1

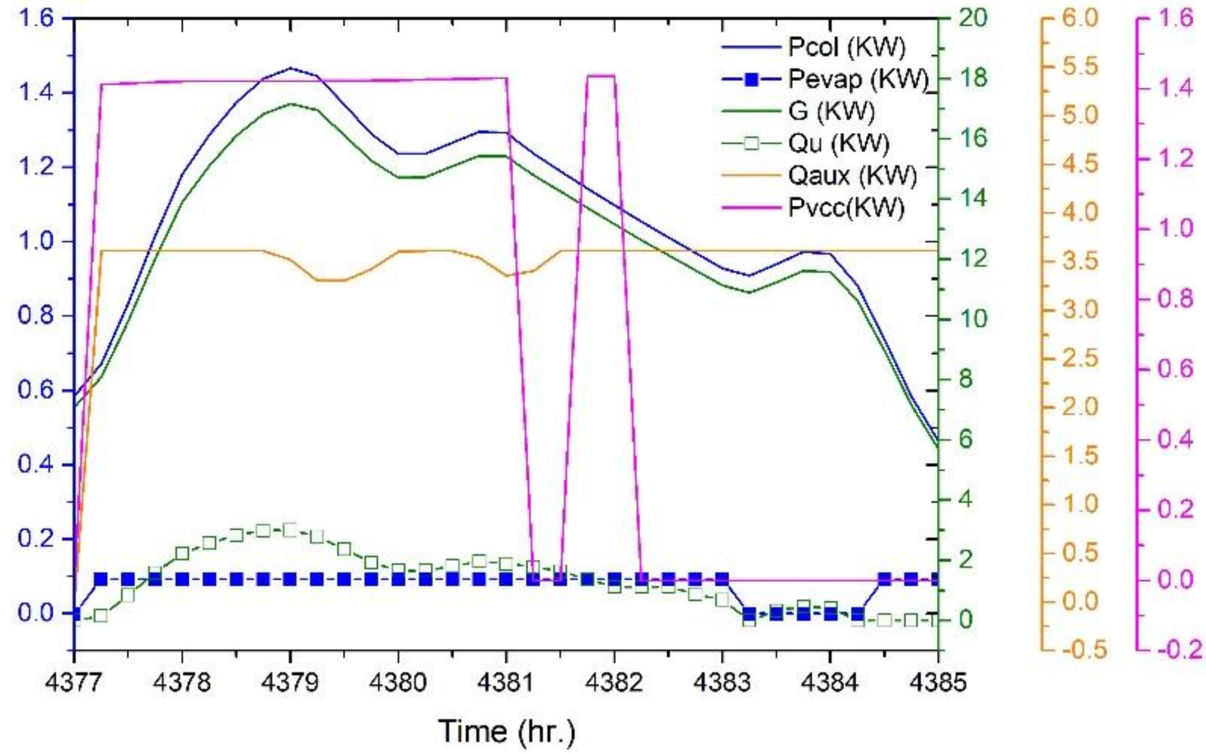

Fig 25: Energy Profile for a Single Day C-2

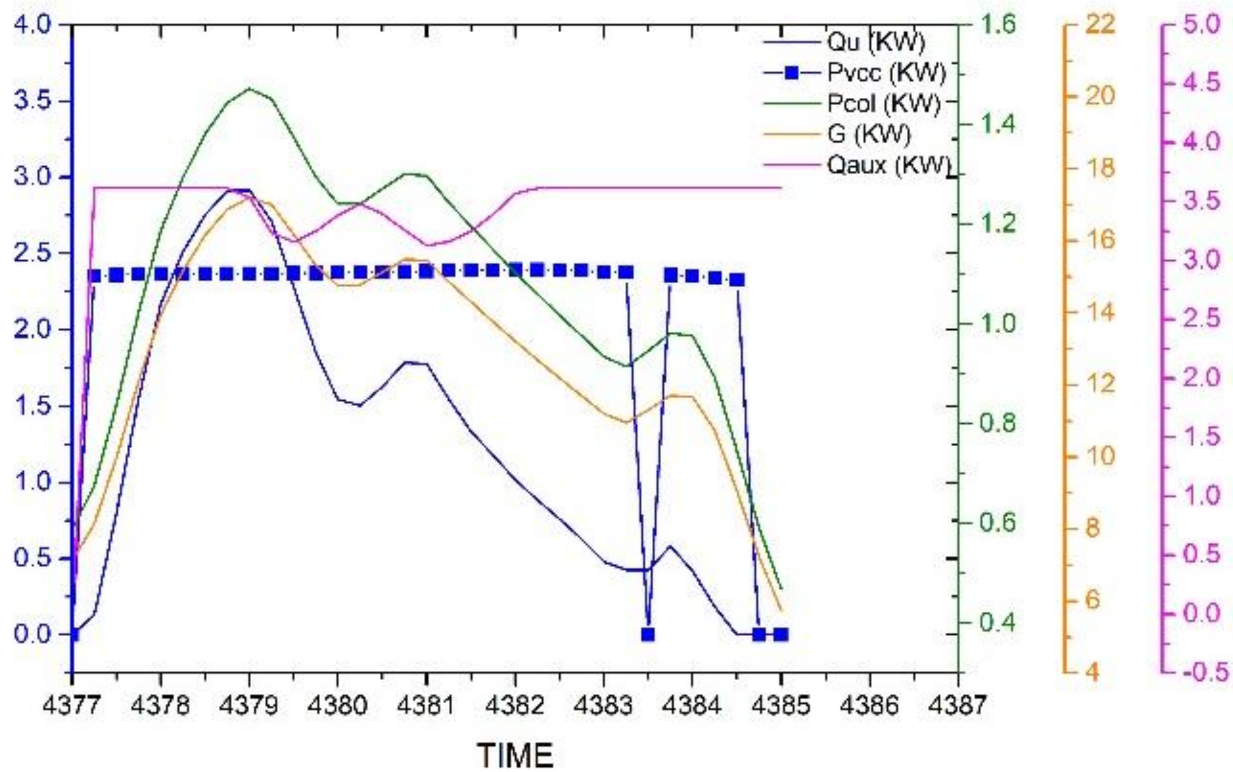

Fig 26: Energy Profile for a Single Day C-3

6. Conclusions

In this study, three configuration schemes of a solar-based desiccant cooling system are modeled and simulated in TRNSYS for the whole summer season based on the weather data for the location of Lahore (31.52° N, 74.36° E). The heat generation loop of the models primarily consists of flat-plate PV/T solar collector, thermal and electric storages, and the auxiliary heater. The air conditioning loop includes desiccant wheel, direct/indirect evaporative coolers, vapor compression chiller, air to air and air to water heat exchangers and a synthetic building load generator with the peak cooling demand of 2.5 TR.

Based on simulations for the whole season, optimum tilt of the solar collector for all configuration schemes are estimated to be 15^{o}. Optimum storage volume for solar collector area of 25 m^2 and for SF_{th} of at least 40 % and above is determined to be 0.6 m^3 for all configuration schemes. Similarly, for achieving SF_{th} of 50 % solar PV/T collector area of ~20 m^2 is estimated for C-1 while 30 m^2 is required for C-2 and C-3. C-3 configuration, due to the absence of evaporative coolers, resulted in significantly lower primary energy savings (f_{sav}) than C-1 and C-2 configurations. The required regeneration temperature of the desiccant wheel showed a considerable influence on f_{sav} and SF_{th} as for the same collector area the increase in regeneration temperature 50 ^{o}C to 70 ^{o}C reduces the f_{sav} by up to 90 % for all configuration schemes.

Overall, C-1 scheme having the auxiliary heater in the return air loop resulted in the highest f_{sav} and SF_{th} amongst all the configuration schemes. C-2 and C-3 schemes with auxiliary heater in the solar water heating loop requires a much higher temperature of the water than in C-1 to heat the return air in the water-air heat exchanger to the required regeneration temperature. Hence, for the same regeneration temperature C-2 and C-3 scheme operates under high temperature in the solar loop and resulted in lower values of collector's thermal efficiency and other thermal performance factors (such as f_{sav}, SF_{th}) than C-1. C-3 scheme with no evaporative coolers in the desiccant loop is not found to be the preferred option for the solar-based system as for a particular solar collector area f_{sav} was estimated to be far too small in comparison to C-1 and C-2 schemes.

Nomenclature

U_L	Overall thermal loss coefficient of the collector per unit area [kJ/h-m²-K]
T_{av}	Average collector fluid temperature [K]
T_a	Ambient temperature [K]
β	Collector slope [degrees]
$m.$	Mass flow rate [kg/hr]

C_P	Specific heat of the fluid [kJ/kg. K]
T_{evap}	Temperature of air entering/exiting the evaporator side of the coil. [K]
Q_{total}	Rate of total energy transferred by the coil [kJ/hr]
$\boldsymbol{\omega}$	Humidity Ratio. [kg H_20/kg Air]
$\boldsymbol{\varepsilon}$	Heat exchanger effectiveness (-)
Q_{aux}	Total rate of energy input from auxiliary source [KJ/hr]
Q_{reject}	Rate of energy rejected by coil to atmosphere [KJ/hr]
PWr_{total}	Total power draw by air conditioner [KJ/hr]
$\dot{Q}_{cooling,}$	Energy for cold provided by a conventional vapor compression refrigeration system [KJ/hr]
ε_{heat}	Efficiency of boiler
ε_{elec}	Efficiency of thermal power plant
Q_u	Thermal energy gain of collector [kW]
A	Total collector area. [m^2]
G	Global solar irradiance on tilted surface [W/m^2]
$\tau\alpha$	Effective transmittance-absorbtance product of the glazing and surface coating of the absorbed plate
T_i	Inlet fluid temperature [K]
T_a	Ambient temperature [K]
T_f	Mean fluid temperature [K]
N_G	Number of glass covers [-]
T_P	Mean absorber plate temperature [K]
h_w	Wind heat transfer co-efficient [-]
β	Collector slope [-]
$\boldsymbol{\varepsilon}_P$	Thermal emittance of plate [-]
$\boldsymbol{\varepsilon}_g$	Thermal emittance of glass [-]
U_{be}	Combined heat loss co-efficient from the bottom and edges of PV-T collector
Q_{sens}	Sensible energy transfer between air streams. [KJ/hr]
$\boldsymbol{\varepsilon}_{sens}$	Sensible effectiveness of the device [-]
C_{min}	Minimum capacitance (mass flow rate times specific heat) air streams.
$T_{return,\, in}$	Temperature of return air [K]
$T_{process,\, in}$	Temperature of process air after passing desiccant wheel [K]
$T_{air,\, o}$	Dry bulb temperature of air exiting the cooling device [K]
$T_{air,\, i}$	Dry bulb temperature of air entering the cooling device [K]
η_{sat}	Saturation efficiency of evaporative cooling process [-]
T_{wbd}	Wet bulb depression (the maximum temperature difference possible between inlet and outlet of dry-bulb air temperature [K]
η_{th}	Thermal efficiency of collector [-]
η_{elec}	Electrical efficiency of collector [-]
SF_{th}	Thermal solar fraction [-]
SF_{elec}	Electrical solar fraction [-]

Q_s	Heat energy provided by solar collector [KW]
Q_b	Heat energy provided by auxiliary boiler [KW]
P_s	Electrical energy provided by solar collector [KW]
P_b	Electrical energy provided by grid source [KW]
$Q_{c,\,ac}$	Cooling energy produced by the conventional air-conditioning unit in a desiccant cooling system [KW]
COP_{ac}	Co-efficient of performance of air-conditioner [-]
$Q_{c,\,acref}$	Total primary energy requirement to run a conventional vapor compression-based air conditioning system to meet the same cooling load [KW]

Abbreviations

PV/T	Photovoltaic-Thermal
C-1	Configuration-1
C-2	Configuration-2
C-3	Configuration-3
VCC	Vapor Compression Chiller
DEC	Direct Evaporative Cooler
Tcol_out	Temperature of water at collector outlet
Tcol_in	Temperature of water at collector inlet
Taux_in	Fluid temperature entering auxiliary boiler
Taux_out	Fluid temperature exiting auxiliary boiler
Tw_wHX_in	Temperature of water entering the water to air heat exchanger
Tw_wHX_out	Temperature of water exiting the water to air heat exchanger
TaaHX_in	Air entering in air to air heat exchanger
TaaHX_out	Air exiting from air to air heat exchanger
Tavap_out	Air exiting from direct evaporative cooler
Tvcc_out	Air exiting from vapor compression chiller
Troom	Room temperature
Tamb	Ambient temperature
Ta_wHX_out	Temperature of air exiting from water to air heat exchanger.
Ta_wHX_in	Temperature of air entering in water to air heat exchanger.
Treg	Temperature of regeneration air

[1] F. Assilzadeh, S. A. Kalogirou, Y. Ali and K. Sopian, "Simulation and optimization of LiBr solar absorption cooling system with evacuated tube collectors.," *Renewable Energy*, vol. 30, pp. 1143-1159, 2005.

[2] Y. Fan, L. Luo and B. Souri, "Review of solid sorption refrigeration technologies:development and

applications," *Renewable and Sustainable Energy Reviews,* vol. 11, pp. 1758-1775, 2007.

[3] A. W. Bhutto, A. A. Bazmi and G. Zahedi, "Greener energy: Issues and challenges for Pakistan—wind power prospective," *Renewable and Sustainable Energy Reviews,* vol. 20, pp. 519-538, 2013.

[4] E. Y. A. C. Naci Kalkan, "Solar thermal air conditioning technology reducing the footprint of solar thermal air conditioning," *Renewable and Sustainable Energy Reviews,* vol. 16, pp. 6352-6383, 2012.

[5] K. Daou, R. Z. Wang and Z. Z. Xia, "Desiccant cooling air conditioning : a review," *Renewable and Sustainable Energy Reviews,* vol. 10, pp. 55-77, 2006.

[6] T. T. R. P. P. Otanicar, "Prospects for solar cooling - an economic and and environmental assessment," *Solar Energy,* no. 86, pp. 1287-1299, 2012.

[7] J. C. Sheridan and J. W. Michell, "A hybrid solar desiccant cooling system," *Solar Energy,* vol. 34, pp. 187-193, 1985.

[8] N. Subramanyam, M. P. Maiya and S. S. Murthy, "Application of desiccant wheel to control humidity in air-conditioning systems," *Applied Thermal Engineering,* no. 24, pp. 2777-2788, 2004.

[9] A.khalid, M. Mehmood, M. Asif and e. al, "Solar assisted, pre-cooled hybrid desiccant cooling system for Pakistan," *Renewable Energy,* no. 1, pp. 151-157, 2009.

[10] A. Alili, Y. Hwang, R. Radermacher and I. Kubo, "A high efficiency solar air conditioner using concentrating photovoltaic/thermal collectors," *Applied Energy,* no. 93, pp. 138-147, 2012.

[11] Q. Ronghui, L. Lin and H. Yu, "Energy performance of solar-assisted liquid desiccant air-conditioning system for commercial building in main climate zones," *Energy Conversion and Management,* vol. 88, pp. 749-757, 2014.

[12] T. S. Ge, Y. J. Dai, R. Z. Wang and Y. Li, "Performance of two-stage rotary desiccant cooling system with different regeneration temperatures," *Energy,* no. 80, pp. 556-566, 2015.

[13] G. Angrisani, F. Minichiello and M. Sasso, "Improvements of an unconventional desiccant air conditioning system based on experimental investigations," *Energy Conversion and Management,* vol. 112, pp. 423-434, 2016.

[14] T. Elmer, M. Worall, S. Wu and S. Riffat, "An experimental study of a novel integrated desiccant air conditioning system for building applications," *Energy and Buildings,* vol. 111, pp. 434-445, 2016.

[15] A. Heidari, R. Roshandel and V. Vakiloroaya, "An innovative solar assisted desiccant-based evaporative cooling system for co-production of water and cooling in hot and humid climates," *Energy Conversion and Management,* pp. 396-409, 1 4 2019.

[16] M. S. Buker, B. Mempouo and S. B. Riffat, "Experimental investigation of a building integrated photovoltaic/thermal roof collector combined with a liquid desiccant enhanced indirect evaporative cooling system," *Energy Conversion and Management,* vol. 101, pp. 239-254, 10 6 2015.

[17] A. W. B. T. T. M. W. K. F. S. B. Muhammad Shoaib Ahmed Khan, "Configuration based modeling and performance analysis of single effect solar absorption cooling system in TRNSYS," *Energy Conversion and Management,* no. 157, pp. 351-363, 2018.

[18] J. M. C.-L. F. D.-M. a. A. C.-A. N. Molero-Villar, "Solar Energy," *A comparison of solar absorption system configurations,* vol. 86, no. 1, pp. 242-252, 2012.

[19] M. Mujahid Rafique, P. Gandhidasan, S. Rehman and L. M. Al-Hadhrami, *A review on desiccant based evaporative cooling systems,* vol. 45, Elsevier Ltd, 2015, pp. 145-159.

[20] W. A. B. John A. Duffie, Wiley: Solar Engineering of Thermal Processes, 4th Edition - John A. Duffie, William A. Beckman, 2013, p. 936.

[21] J. Jurinak, "Open Cycle Desiccant Cooling – Component Models and System Simulations," PhD Thesis, University of Wisconsin, Medison, 1982.

[22] R. Howe, "Model and Performance Characteristics of a Commercially-Sized Hybrid Air Conditioning System Which Utilizes a Rotary Desiccant Dehumidifier," MS Thesis, University of Wisconsin, Madison, 1983.

[23] *TRNSYS 18: A transient simulation program,* Madison, USA: SOlar Energy Laboratory, University of Wisconsin.

[24] K. F. Fong, T. T. Chow, C. K. Lee, Z. Lin and L. S. Chan, "comparative study of different solar cooling systems for buildings in subtropical city," *Solar Energy,* vol. 84, no. 2, pp. 227-244, 2010.

[25] W. Sparber, A. Thuer, F. Besana, W. Streicher and W. Streicher, "Unified Monitoring Procedure and

Performance Assessment for Solar," in *1st International Conference on Solar Heating, Cooling and Buildings.*, Lisbon, 2008.

[26] M. G. A. C. Robert Foster, Solar Energy: Renewable Energy and the Environment, Boca Raton: Taylor and Francis Group, 2010.

[27] S. A. G. B. Ali Alahmera, "Effect of parameters on moisture removal capacity in the desiccant," *Case Studies in Thermal Engineering,* no. 13, 2019.